UNIVERSITY OF THESSALY
SCHOOL OF ENGINEERING
DEPARTMENT OF MECHANICAL ENGINEERING

ROBUST PREDICTION OF FATIGUE DAMAGE ACCUMULATION IN METALLIC STRUCTURES USING OUTPUT-ONLY VIBRATION MEASUREMENTS

SYSTEM DYNAMICS LABORATORY

Diploma Thesis by

DIMITRIOS GEORGIOS FISTES

In partial fulfillment of requirements

for the diploma degree

July 2017

Thesis Committee

Costas Papadimitriou

Professor of Structural Dynamics, Department of Mechanical Engineering, University of Thessaly.

Nikolaos Aravas

Professor of Computational Mechanics, Department of Mechanical Engineering, University of Thessaly.

Dimitrios Giagkopoulos

Assistant Professor of Structural Dynamics, Department of Mechanical Engineering, University of Western Macedonian.

SUMMARY

The subject of the current diploma thesis is the development of methods that predict the fatigue damage accumulation of any metallic structure using a limited number of response time histories. For this, a dual Kalman filter (DKF) is used. It is shown that using acceleration and displacement measurements from a limited number of degrees of freedom it is possible to predict the acceleration, displacement, force, strain and stress time histories all over the structure using the DKF. In order to take excellent predictions, tuning methods for the covariance matrices of observation, load and state are studied and presented. The strain predictions that are taken from the DKF are used in order to calculate the stresses all over the structure. After that, the fatigue damage accumulation and lifetime is calculated for the metallic structure and decisions are taken for the safety of the system. Furthermore, emphasis is given on the model uncertainties and their effects on the acceleration, displacement and strain prediction and lifetime prognosis. After that, a metallic base from the power plant of AHS Melitis in Florina is studied and the dual Kalman filter approach is applied. Using acceleration measurements from some DOFS of the system it will be shown that it is possible to predict the unknown force, displacement and acceleration time histories everywhere in the system. The second part of diploma thesis herein is concerned with the optimal location and the appropriate number of sensors which are used, in order to take excellent predictions in the DKF. Also it is assumed that there are different kinds of uncertainties, which are also studied herein.

LIST OF CONTENTS

LIST OF FIGURES

LIST OF TABLES

ACKNOWLEDGEMENTS

First of all I would like to express my gratitude to my supervisor Prof. Costas Papadimitriou for the useful comments, remarks and guidance through the learning process of this diploma thesis. Furthermore, I would like to thank Postdoctoral Researcher Saeed Eftekhar Azam of Politecnico di Milano for introducing me to the topic of Dual Kalman Filter and his support on the way. Additionally, I would like to thank Assistant Professor Dimitrios Giagkopoulos of University of Western Macedonian for his patience and his useful advice all these months. Finally, I would like to thank Prof. N. Aravas and Assistant Professor Dimitrios Giagkopoulos for serving in my thesis committee.

This thesis is dedicated to my father and my mother

CHAPTER 1 Introduction

1.1 Content of the diploma thesis

The oscillation of dynamic systems due to external excitations such as wind and earthquake is a very important issue for the safety of the mechanical structures and the protection of the people who use these structures. Nowadays, the large development of the technology results in the evolution of accurate computational models and reliable simulations techniques which can analyze complicated dynamic systems and predict fatigue damage accumulation of many complex metallic structures such as buildings, bridges and turbines etc.

At first, the diploma thesis herein is dealing with the prediction of acceleration and displacement time histories in every spot of a linear spring-mass chain-like model, by using the Dual Kalman Filter technique. Note that the input load of the system is unknown and that acceleration measurements are taken from a sensor network attached to the structure. This type of filter is used by Eftekhar Azam, Chatzi and Papadimitriou for state estimation by using only acceleration measurements [1] and by Eftekhar Azam, Chatzi and Papadimitriou in experimental validation of the Kalman-type filters for online and real-time state and input estimation. Kalman Filter techniques have also studied from Lourens and Papadimitriou, who used a Kalman filter technique for jointly estimating the input and state of a structure from a limited number of acceleration measurements [14] and from Papadimitriou and Fritzen [3]. For nonlinear models the extended Kalman filter is used. The work of S. Mariani and A. Ghisi has been study and examined [31].

An important issue is the selection of the values of the covariance matrices, which depends on the model of the system. Unfortunately, the computational models and the results from the simulations will be incorrect due to the drift effect, if appropriate values for the covariance of the process noise and the covariance of input force are not chosen carefully. This crucial section of the Kalman Filter has been studied from Bittanti and Savaresi [7] and Rajamani and Rawlings [8]. In the last years, there are important studies for automatically tuning the covariances of process and observation noise in Kontoroupi and Smyth [26].

In addition, another problem that arises from the study of a dynamic system is that there may be some uncertainties that are associated with the model of the system. These uncertainties are usually arising due to simplified assumptions made by the analyst concerning the choice of elements, the behavior of the structure, the loads that are applied on the structure etc. Furthermore, there are uncertainties that are correlated with the stiffness of the material, the damping ratio and the mass of the model. Generally, there are three types of uncertainties:

- Modeling uncertainties: uncertainties due to the behavior of materials, friction mechanism, the type of material processing etc.

- Loading uncertainties: uncertainties that arise due to the behavior of the applied force, the dynamics of the structures in detail, spatial and temporal variability of earthquake induced excitations on civil engineering structures, turbulent wind loads affecting the design of aircrafts etc.
- Numerical uncertainties: rounding-off errors in numerical solutions due to computer inaccuracies.

In this diploma thesis emphasis is given on the model uncertainties; namely, uncertainties that are related to the stiffness of the material are examined.
As it is mentioned above, the fatigue damage accumulation for the entire examined structure is very important for maintenance strategies. The predicted strain time histories for all the hotspots locations of the structure are used to calculate the stress response time histories in the entire body of the structure using the output-only vibration measurements. Recombining the predicted stress time histories, the linear Palmgren-Miner damage accumulation law [27],[28], S-N curves and stress cycle counting method, such as the Rainflow cycle-counting method it is easy to predict the fatigue damage accumulation for a structure and find the crucial and most dangerous hotspots of the system. Here it must be emphasized again the important role of the Dual Kalman Filter to this study since having limited sensor network, it is possible to obtain measurements of the stress time history and thus the fatigue at all hotspot locations of the structure. Using the DKF it is possible to take predictions from all over the structure. Important study in this field has been done by Papadimitriou & Fritzen [3], Lourens, Papadimitriou, Lombaert, Roeck & Liu [22].

In addition another important issue that it is studied herein is how to choose the optimal location for the sensors in the examined structure. This part of the study is very crucial because by finding the optimal sensor placement in structural dynamics one can minimize the error in the predictions made using the information in the measurements. Previous studies in this field have been done by F. E. Udwadia [20], C. Papadimitriou [18] and Eric Hernandez [21]. Moreover, in this diploma thesis the effects of different types of model uncertainties on the optimal selection of the sensors' location are studied, since the quality of the information that it is taken from the measurements depends on the model (Papadimitriou [18]).

A real-life example is studied in Chapter 6. Using acceleration measurements from a limited number of sensors located on some points of the system it is possible to make predictions for the acceleration, displacement and unknown force time histories for all the DOFS of the system using the DKF. The stiffness, mass and damping matrices as well as the measurements are taken by studying the work of D. Giagopoulos et all in the paper [32]. First, in the aforementioned paper, a discrete model of steel base is developed. The DKF use information from a high fidelity FE model of the structure. Additionally, measured FRFs are used for estimating the natural frequencies and the damping ratios of the system. Structural identification methods are used for estimating the parameters of the FE model, based on minimizing the discrepancy between the experimental and analytical modal characteristics, in order to develop a high fidelity FE model. To optimize the FE model of the structure, structural model updating methods

have been proposed in order to reconcile the numerical FE model with experimental data.

It is assumed that passive systems include a primary 10-DOF spring-mass chain like model and a secondary 1-DOF spring-mass chain like model. The secondary system is attached on the primary system in a certain location and a general spring mass system is created. In the context of this diploma thesis the effects that the secondary system and its uncertainties have on the optimal sensor placement will be studied and discussed.

1.2 Organization of the diploma thesis

In this diploma thesis the following different areas of research are studied:

(1) The mathematical presentation of the dual Kalman Filter for predicting accelerations displacements and strains in various structural locations using acceleration, displacement and strain measurements at a limited number of structural locations. The appropriate formulations of the covariances of noise and state are covered in Chapter 2.

(2) The study of uncertainties in dual Kalman filter for a spring-mass chain-like model is presented in Chapter 3 and the study and the effects of uncertainties in fatigue damage accumulation for the system in Chapter 4

(3) The optimal sensor placement and the effects of different types of uncertainties are studying in the first part of Chapter 5. In the second part of Chapter 5 the effects of the secondary system on the optimal sensor placement are studied and different kinds of uncertainties are examined.

(4) The effectiveness of the Dual Kalman Filter for predictions of acceleration, displacement and unknown force time histories for a metallic base from Meliti PPC power plant are investigated in Chapter 6.

CHAPTER 2 A Dual Kalman Filter Approach with Unknown Input Force

2.1 Mathematical formulation of the problem-Theoretical approach

Consider the linear structural dynamics problem that is formulated using the following continuous time second order equation discretized in space

$$\mathbf{M\ddot{u}(t) + C\dot{u}(t) + Ku(t) = f(t) = S_p(t)p(t),} \quad \textbf{(1)}$$

where **u (t)** is a matrix ϵR^{nxn} stands for the displacement, **K**, **M** and **C** ϵR^{nxn} are symmetric matrices that stand for stiffness ,damping and mass respectively. The **n** symbol stands for the degrees of freedom of the system. The vector **f (t)** is defined as the excitation force. Also, the influence matrix $\mathbf{S_p(t)}$ ϵR^{npxn} gives the distribution of the load time history in some degrees of freedom on the structure . Finally, **p (t)** is the time history of the load.

To solve the aforementioned equation, consider the eigenvalue problem $\mathbf{K\Phi = M\Phi\Omega^2}$**.** Also the orthogonality equations $\mathbf{\Phi^T M\Phi = I}$, $\mathbf{\Phi^T K\Phi = \Omega^2}$ and $\mathbf{\Phi^T C\Phi = \Gamma}$ are used, where $\mathbf{\Phi}$ ϵR^{nxn} is a matrix containing the eigenvectors Φ_i for each degree of freedom , $\mathbf{\Omega}$ ϵR^{nxn} is a diagonal matrix containing the eigenfrequencies, $\mathbf{\Gamma} \epsilon R^{nxn}$is a diagonal matrix with $2\xi_i\omega_i$ diagonal components and ξ_i stands for the modal damping ratio of each degree of freedom. Furthermore by introducing the coordinate transformation **u(t)=Φz(t)** ,the equation (1) becomes

$$\mathbf{\Phi^T M\Phi\ddot{z}(t) + \Phi^T C\Phi\dot{z}(t) + \Phi^T K\Phi z(t) = \Phi^T S_p(t)p(t)} \quad \textbf{(2)}$$

Using the aforementioned orthogonality conditions, the equation above is transformed to

$$\mathbf{\ddot{z}(t) + \Gamma\dot{z}(t) + \Omega^2 z(t) = \Phi^T S_p(t)p(t)} \quad \textbf{(3)}$$

Introducing the state vector **x(t)=[u(t) u̇(t)]**, with **x(t)** ϵR^{2nx2n} the equation (1) can be transformed into a first order continuous-time state equation

$$\mathbf{\dot{x}(t) = A_c x(t) + B_c p(t)} \quad \textbf{(4)}$$

where $\mathbf{A_c}$ ϵR^{2nx2n} and $\mathbf{B_c}$ ϵR^{2nxnp} are the following matrices

$$\mathbf{A_c} = \begin{bmatrix} \mathbf{0} & \mathbf{I} \\ -\mathbf{K/M} & -\mathbf{C/M} \end{bmatrix}$$

$$\mathbf{B_c} = \begin{bmatrix} \mathbf{0} \\ -\mathbf{S_p M^{-1}} \end{bmatrix}$$

The measurements of the displacement, velocity and acceleration are imported in the system through the measurement vector **d(t)** $\epsilon R^{n_o x 1}$

$$\mathbf{d(t) = S_a\ddot{u}(t) + S_v\dot{u}(t) + S_d u(t)} \quad \textbf{(5)}$$

where $\mathbf{S_a, S_d, S_v} \in \mathrm{R}^{n_d x n}$ are selection matrices for acceleration, displacement and velocity respectively. The parameter n_d stands for the number of acceleration, displacement or velocity measurements. These matrices are used to identify the degrees of freedom where the measurements are taken. In this diploma thesis acceleration measurements are usually used.

It follows that the state-space form of the equation (5) is given by

$$\mathbf{d(t) = G_c x(t) + J_c p(t)} \qquad \mathbf{(6)}$$

where the matrices $\mathbf{G_c} \in \mathrm{R}^{n_d x 2n}$ and $\mathbf{J_c} \in \mathrm{R}^{n_d x n_p}$ are defined as

$\mathbf{G_c = [S_d - S_a M^{-1} K \; S_v - S_a M^{-1} C]}$ and

$\mathbf{J_c = [S_a M^{-1} S_p]}$

Note that the combination of equations (4) and (6) gives the continuous-time state –space model for the equation of motion (1). If a reduced order state-space model is needed, the modal analysis is taken place and the following transformation must be done

$$x(t) = \begin{bmatrix} \Phi_r & 0 \\ 0 & \Phi_r \end{bmatrix} \zeta(t)$$

where $\zeta(t) \in \mathrm{R}^{2m}$ is the reduced state for the m modes, m is the number of modes that are used in the analysis and $\Phi_r \in \mathrm{R}^{nx1}$ are the eigenvectors of the modes. Here, the reduced modal state vector $z(t) \in \mathrm{R}^{m}$ is introduced ,where

$$\zeta(t) = \begin{bmatrix} z(t) \\ \dot{z}(t) \end{bmatrix}$$

As a result, the continuous-time state-space equation could take the following reduced order form

$$\dot{\zeta}(t) = A_c \zeta(t) + B_c p(t)$$

$$d(t) = G_c \zeta(t) + J_c p(t)$$

We can prove that the four matrices above have the following form

$$A_c = \begin{bmatrix} 0 & I \\ -\Omega^2 & -\Gamma \end{bmatrix},$$

$$B_c = \begin{bmatrix} 0 \\ -S_p \Phi^T \end{bmatrix},$$

$$G_c = \begin{bmatrix} S_d \Phi_r & 0 \\ 0 & S_v \Phi_r \\ S_a \Phi_r \Omega^2 & S_a \Phi_r \Gamma \end{bmatrix},$$

$$J_c = \begin{bmatrix} 0 \\ 0 \\ S_a \Phi_r \Phi_r^T S_p \end{bmatrix}$$

Under the assumption that the sampling rate is 1/dt, the continuous time equations (4) ,(6) can be discretized in time as follows :

$\mathbf{x_{k+1}= Ax_k + Bp_k + w_k}$

$\mathbf{d_k= Gx_k + Jp_k + v_k}$

where $\mathbf{A= e^{A_c dt}}$, $\mathbf{B=[A-I]A_c^{-1}B_c}$, $\mathbf{G_c = G}$, $\mathbf{J_c = J}$ and $\mathbf{x_k=x(kdt)}$, $\mathbf{p_k = p(kdt)}$, $\mathbf{d_k= d(kdt)}$, assuming that k=1,…,N. Hence, N is equal to T/dt. The **J** is the direct transmission matrix and **G** is the output influence matrix. Furthermore, $\mathbf{w_k}$ and $\mathbf{v_k}$ are random vectors for the stochastic system and measurement noise respectively. We assume that these two aforementioned vectors are mutually uncorrelated, zero mean and white Gaussian noise processes with the following covariance matrices $Q=E[w_k w_k^T]$ and $R= [v_k v_k^T]$.

2.2 Algorithm of the Dual Kalman filter and state estimation

In this section, a dual Kalman filter is proposed in order to estimate the partially observed state x_k. Let's take the aforementioned discrete-time state space equation

$\mathbf{x_{k+1}= Ax_k + Bp_k + v_k^x}$

$\mathbf{d_k= Gx_k + Jp_k + w_k}$ **(7)**

Regarding the state space form of the unknown force, we introduce

$\mathbf{p_{k+1}= p_k + v^p_k}$ **(8)**

where v^p_k is zero mean and white, with Q^p covariance matrix.

Combining the equations (7) and (8) a new state-space equation can be obtained

$\mathbf{p_{k+1}= p_k + v^p_k}$ **(9)**

$\mathbf{d_k= Gx_k + Jp_k + w_k}$ **(10)**

By using the equation (9) the unknown force could be calculated and then, by recombining equations (7) and (8) we could estimate the unknown state x_k. It is assumed that the input p_k is unknown, but the observation vector d_k can be calculated if the equation (5) is taken into account. At this point, a two-stage Kalman filter is introduced, based on the filter proposed on S. Eftekhar Azam et al [1]. The first part is the stage for estimating the unknown input force and the second is the stage for the predicting and updating the observed state x_k. At first the algorithm deals with the calculation of the input force. The first move is to initialize the state estimate $\hat{\mathbf{x}}$ and the error covariance matrix of the state $\mathbf{P^x_0}$, where

$\hat{x}_0= E[\hat{x}_0]$ and

$P^x_0= E[(x_k - \widehat{x_k})(x_k - \widehat{x_k})^T]$

With the same procedure, the input estimate $\hat{\mathbf{p}}$ and its covariance $\mathbf{P^p_0}$ are initialized

$\hat{p}_0= E[p_0]$ and

$P^{p}_{0}=E\,[(p_0 - \hat{p}_0)(p_0 - \hat{p}_0)^T]$

It follows the *second step* of this algorithm, the prediction stage for the input, where

$p^{-}_{k}= p_{k-1}$

$P^{p-}_{k}=P^{p}_{k-1} + Q^{p}$

Furthermore, the *last step* for the input is the update stage, where the Kalman gain for input is calculated

$G^{p}_{k}= P^{p-}_{k} J^T(JP^{p-}_{k}J^T+R)^{-1}$

and also the predictions of input are improved, using the latest observation

$\hat{p}_k=p^{-}_{k} + G^{p}_{k}\,(d_k -G\hat{x}_{k-1}-Jp^{-}_{k})$

$P^{p}_{k}= P^{p-}_{k} - G^{p}_{k}\,JP^{p-}_{k}$

It follows the prediction stage for the state and for the error covariance

$x^{-}_{k}= A\hat{x}_{k-1} + B\hat{p}_k$

$P^{-}_{k}=AP_{k-1}A^T+Q^{x}$

And the calculation of Kalman gain for state

$G^{x}_{k}=P^{-}_{k}G^T\,(GP^{-}_{k}G^T +R)^{-1}$

Finally, the last step of the Dual Kalman filter procedure is to improve the predictions of state using latest observation:

$\hat{x}_k= x^{-}_{k} + G^{x}_{k}\,(d_k- Gx^{-}_{k} -J\hat{p}_k)$

The same procedure is done for the covariance of the state

$P_k= P^{-}_{k} - G^{x}_{k}GP^{-}_{k}$

2.3 Simulated example of the dual Kalman filter using only acceleration data

At this point, the effectiveness of the DKF is illustrated using a 10 DOF spring-mass chain-like model. Also, the input forces are assumed unknown, and the states, forces and accelerations are jointly estimated from experimental acceleration data for all the degrees of freedom of the system. The experimental acceleration data are simulated from an algorithm that uses force input time histories. Modal damping is set to 5%, the nominal mass for every degree of freedom is 0.35 *kg* and the nominal stiffness is set to 650 *N/m.* The diagonal components of covariances matrices are set to Q^{p}=0.01, Q^{x}=10^{-27} and R=0.0005. It is assumed that Q^{p} and Q^{x} are equal to the initial values of the covariance of input and state. Acceleration measurements are taken from the 3 & 7 DOF and the unknown input force is applied on 3 & 7 DOF.

Next, the natural frequencies of the 10 modes of a 10-DOF model are represented in the following table after the simulation. Regarding the measurements, let us consider that only acceleration measurements of the response of the structure at the masses are available

Number of Mode	Frequency (Hz)
1	1.0251
2	3.0524
3	5.0115
4	6.8587
5	8.5527
6	10.0556
7	11.3339
8	12.3590
9	13.1080
10	13.5642

Table 2.1: The eigenvalues of the 10-DOF model.

The spectral analysis for the two acceleration measurements from 3 & 7 DOF is presented in Figures 2.1 & 2.2, one for each measurement.

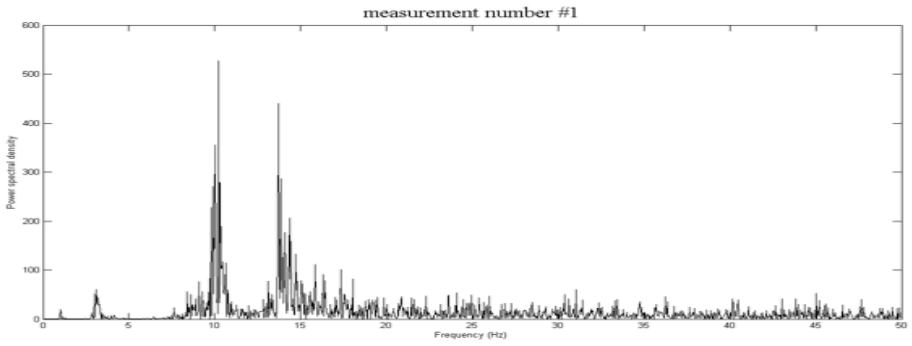

Figure 2.1: Spectrum of the acceleration measurement at 3rd DOF.

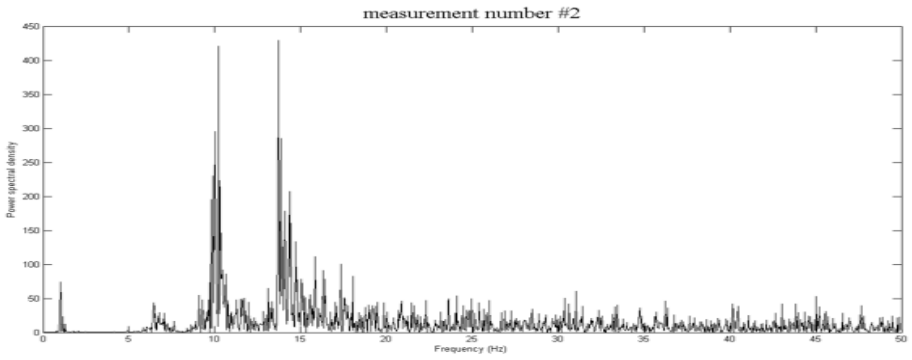

Figure 2.2: Spectrum of the acceleration measurement at 7th DOF.

As it is shown in Figure 2.1 & Figure 2.2 some of the modes are influenced by the acceleration measurements. These modes will determine how the system will move.

Simulated data of the DKF is generated for two cases. **In the first case**, the problem is simulated by solving the typical second order differential equation **(1)** using the matrices K, M and C. **In the second case**, one could use only few modes from the model by using the equation (3) and the eigenvalues, the eigenvectors and the damping ratio of the problem. Displacement predictions for all the DOFS of the model are taken using the conversion $u(t)=\Phi z(t)$. At the end of the simulations, responses of the acceleration, force and displacement are available for all degrees of freedom, regardless of where the measures are taken. Furthermore, at the end of the section, a comparison between the first and the second case is performed, in order to analyze any possible variation.

The test was performed without uncertainties. It is assumed, that the unknown force is applied to the third and seventh degree of freedom.

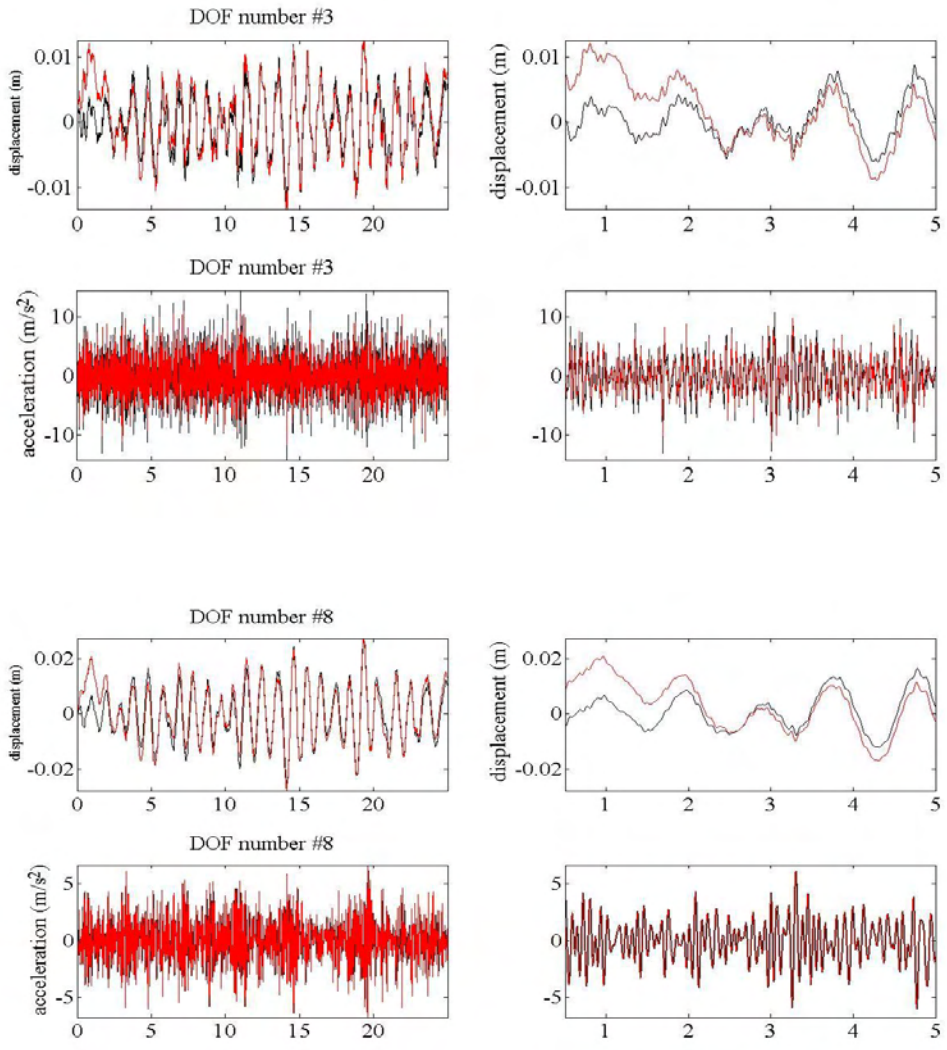

Figure 2.3: Time histories for t=0-25 sec, for the **first case,** when the measures are taken from the third and the seventh dof.

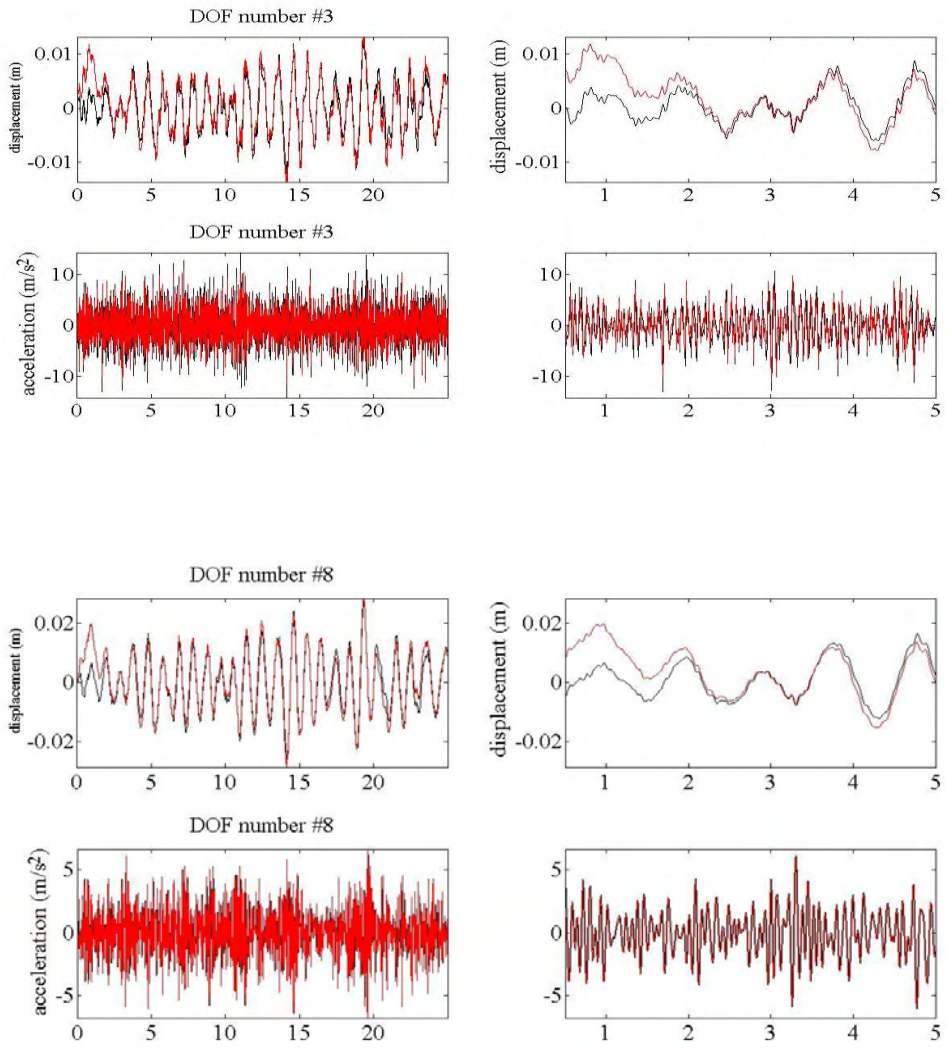

Figure 2.4: Time histories for t=0-25 sec, for the **second case,** when the measures are taken from the third and the seventh dof.

The results of the acceleration and displacement time histories are plotted in Figure 2.3 & 2.4 for two unmeasured location of the model. It can be seen from the comparison of Figures 2.3 and 2.4, that the results of the acceleration and displacement time histories are the same for the two cases. As a result, one can take the same outcome from the DKF, regardless the case that he will use to solve the problem. Note that solving the problem with the second case, one can take the same predictions for acceleration, displacement and force in less simulation time. Moreover, as shown in Figure 2.3 and 2.4, there are some anomalies in the acceleration time histories for the third DOF. This is because the unknown input force location is applied to the third DOF. It is seen that the results that are obtained from the DKF procedure for unmeasured locations are matching good enough with the experimental time histories, as one can see from the aforementioned figures. Despite this, low drifts are observed mainly in the first 2 seconds of the displacement time histories. This problem is studied in another section of the thesis.

Furthermore, the prediction of the unknown applied force is shown in Figure 2.5. The unknown input force is applied to the 3 & 7 DOF of the spring-mass chain like model. It is assumed that the experimental force which is applied to the model is random.

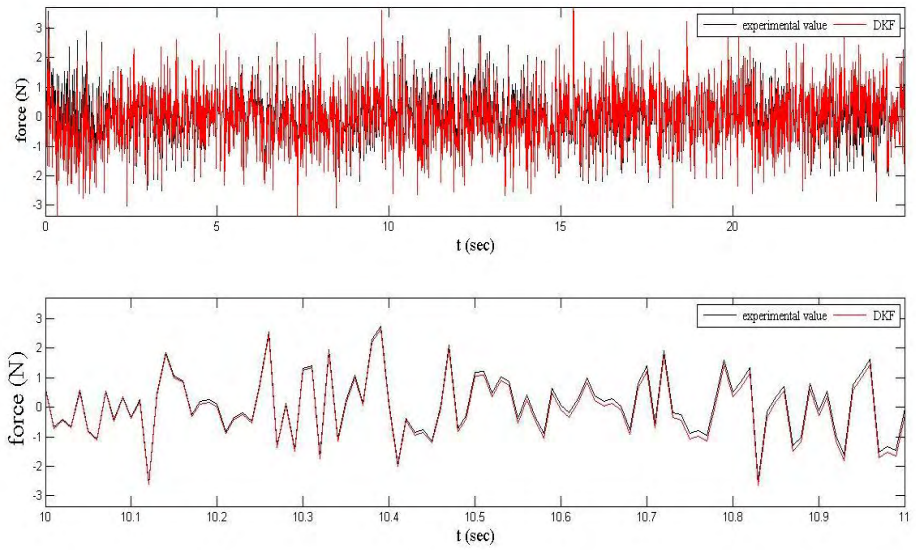

Figure 2.5: Force time history for t=0-25 sec, when the measures are taken from the third and the seventh DOF.

It is seen in Figure 2.5 that, the input force estimation time histories has minimum drifts and it is very accurate with experimental force time histories. As a result, one can conclude that the dual Kalman filter is a very useful and accurate tool in prediction of the unknown input force.

2.4 Simulated example of the dual Kalman filter using displacement and acceleration data

In the last paragraph of this chapter, the dual Kalman filter is used in order to predict the unknown force, acceleration and displacement time histories all over the system using acceleration data from two DOFS of the system. Here, the same model and parameters of the system are used in order to take results using displacement and acceleration data from the 5 DOF and the 3 & 7 DOF respectively. The unknown force is also applied on the 3, 5 and 7 DOFS of the system. The predicted acceleration and displacement time histories for some DOFS are compared with the experimental time histories in Figure 2.6.

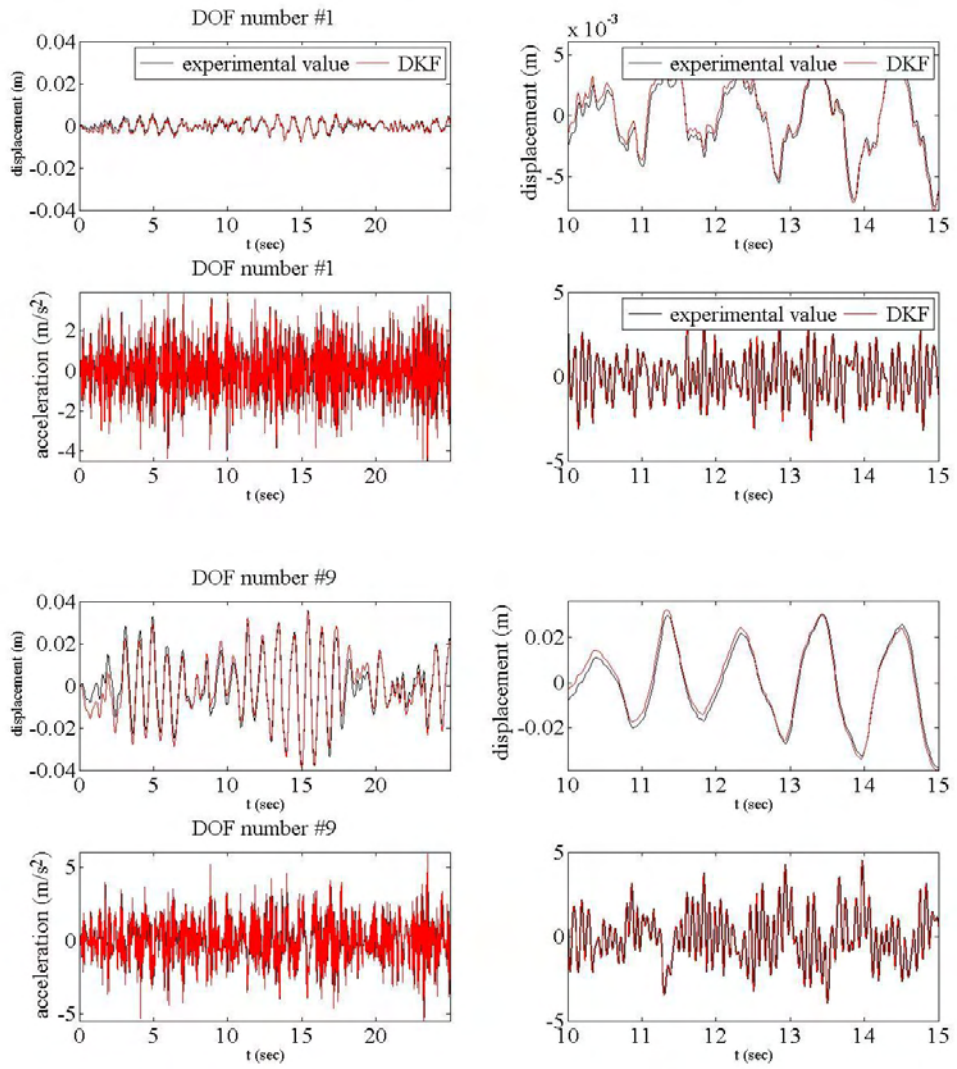

Figure 2.6: acceleration and displacement time histories for two unmeasured location of the model. Comparison between the predicted and experimental time histories is taken place.

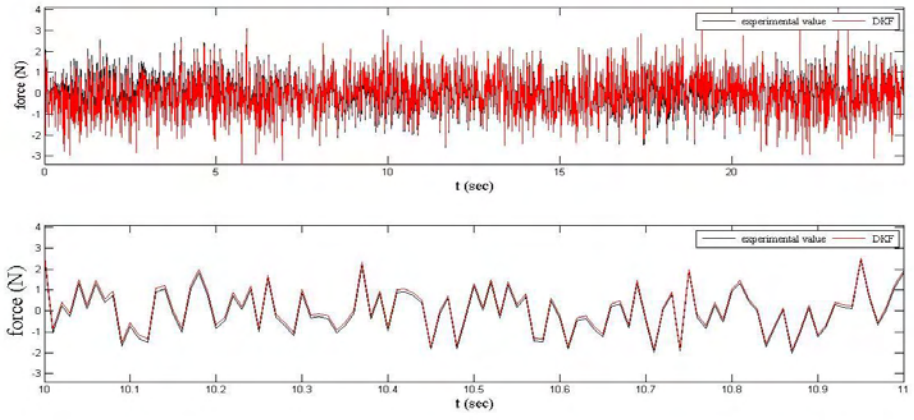

Figure 2.7: prediction of the unknown input force.

For the case that one can have acceleration and displacement measurements the predictions are very satisfying. Namely, in Figure 2.6 one could see that there is a low drift for the first seconds of the simulation. As the time goes by, these drifts are minimized and the predicted acceleration and displacement time histories coincide with the experimental time histories. In Figure 2.7 one could see that the prediction of the unknown applied force is very accurate.

2.5 Estimation of the noise covariance matrices

The objective of this part is to study and demonstrate the influence of the noise covariance matrices Q^x, Q^P, R. For this, it is vital to remind the following equations:

$x_{k+1}= Ax_k + Bp_k + v^x_k$

$d_k= Gx_k + Jp_k + w_k$

where v^x_k and w_k are assumed to be white, mutually uncorrelated stochastic processes, zero mean with covariance matrix Q^x and R respectively, where $Q^x\delta_{kl}=E[w_kw_l]$ and $R\delta_{kl}=E[v_kv_l]$. Also, the unknown input force is following the form

$p_{k+1}=p_k + v^p_k$

where v^p_k is a zero mean white Gaussian process with covariance matrix Q^P.

The diagonal elements of the covariance matrices Q^x, Q^P, R must be chosen deliberately in order to take excellent estimations for the accelerations, displacement and force time histories by disappearing the drifts in the estimates. That's why it is important to make the tuning knob of the system. It is well known that the lower the process covariance matrix is, the more accurate the model is consider to be.

2.6 Simulated example

It follows the estimation of the mean square error **MSE=**$\sum\|\mathbf{d_k} - \mathbf{Gx_k^-} - \mathbf{J\widehat{p_k}}\|_2^2$ **/Nt** of the measure and the prediction of the acceleration time histories in the Dual Kalman Filter for different values of the Q^x, Q^P, R. The model that it is used is a 10 DOF spring-mass chain-like model with k=650 N/m, m=0.35 kg and damping ratio=5%. Thereby, the effects of the fluctuation of the covariance matrices on the predicted acceleration time histories will be shown.

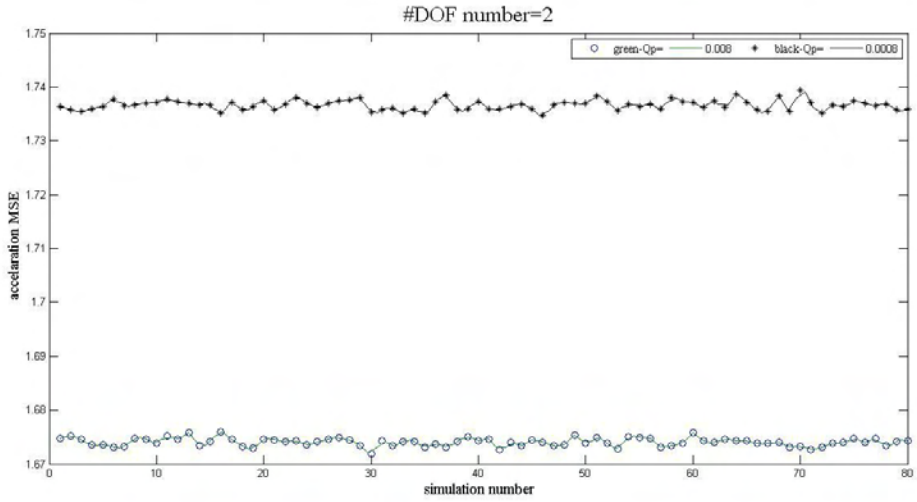

Figure 2.8: 80 simulations for two different values of the diagonal components of input (Q^p) and the effects on the acceleration of the DOF=2.

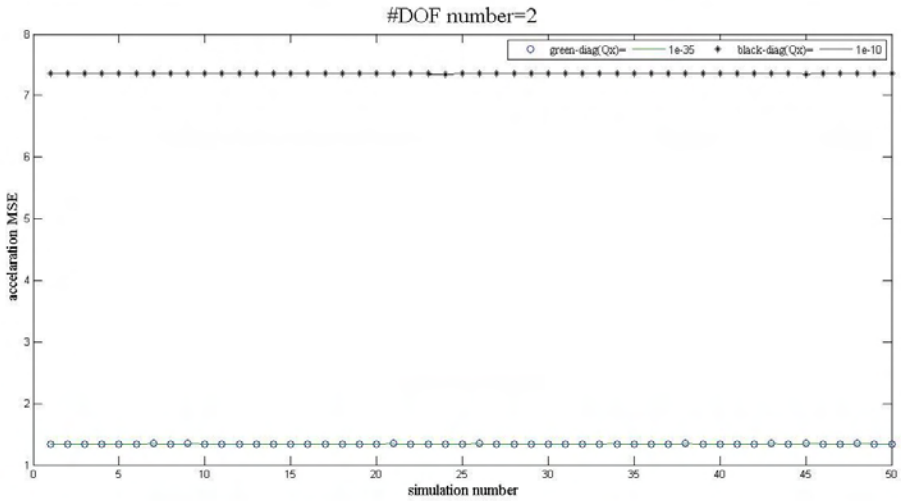

Figure 2.9: 50 simulations for two different values of the diagonal components of state (Q^x) and the effects on the acceleration of the DOF=2.

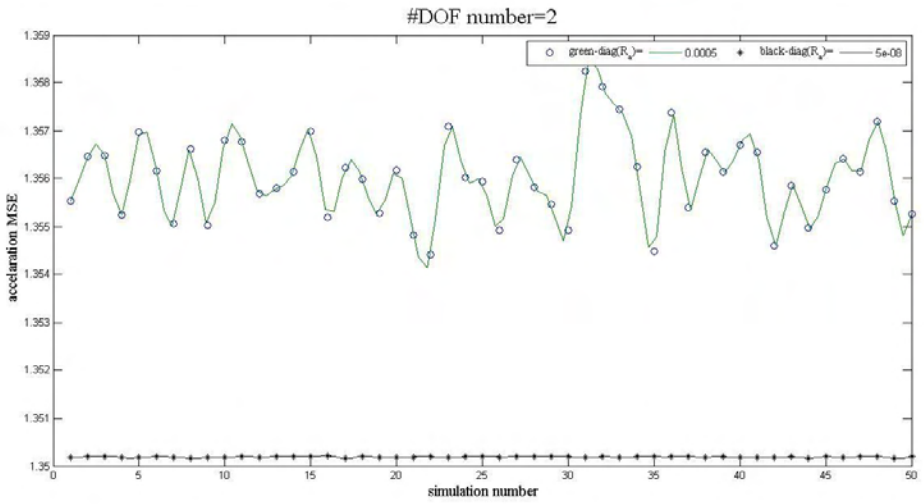

Figure 2.10: 50 simulations for two different values of the diagonal components of the observation noise (R) and the effects on the acceleration of the DOF=2.

Figure 2.8 shows that after 80 simulations, the MSE is increased when the value of Q^P is decreased from Q^P=0.008 to Q^P=0.0008. In Figure 2.9 it is found that when the value of the covariance Q^x is decreased from $Q^x=10^{-10}$ to $Q^x=10^{-35}$, the values of the acceleration MSE are increasing. On the contrary, Figure 2.10 shows the reduction of the MSE values after 50 simulations, while the diagonal components of observation noise covariance are decreasing from R=0.0005 to $R=5*10^{-8}$.

After studying the effects of tuning the covariance matrices, the values of the matrices are chosen as following, $Q^x=10^{-60}$, Q^P=0.008, R=0.0005.

2.7 Tuning the covariance matrices

In this section, a methodology for tuning the covariance matrices is proposed. It is reminded, that in previous sections the problem of determine the appropriate covariance matrices was faced. In order to choose proper values for the covariance of input, the L-curve is used. A 10-DOF spring mass model is used and acceleration measurements are taken from the 2nd DOF. Also it is assumed that the unknown force is applied on the 2nd DOF. The first step is to calculate the mean square error $\mathbf{MSE} = \frac{1}{N_t}\sum_{k=1}^{N_t} //\mathbf{d_k} - \mathbf{G}\mathbf{x}_\mathbf{k}^- - \mathbf{J}\hat{\mathbf{p}}_\mathbf{k}//_2^2$, where d_k are the acceleration measurements of the measured DOFS, N_t are the points of the acceleration time histories and the terminal $Gx_k^- + J\hat{p}_k$ is the prediction of acceleration time histories using the dual Kalman filter procedure. The MSE is calculated using DKF for the acceleration time history of the 2nd DOF, for different values of the covariance input matrix Q^p. Note that the L-curve technique is used only for the DOFS where measurements are taken. Input covariance amplitude between 10^{20} and 10^{-20} is studied, and the results are presented in Figure 2.11. The turning point in L-curve is chosen to be the best option for the Q^P initial value. It is assumed that the diagonal components of Q^x are set 10^{-60}.

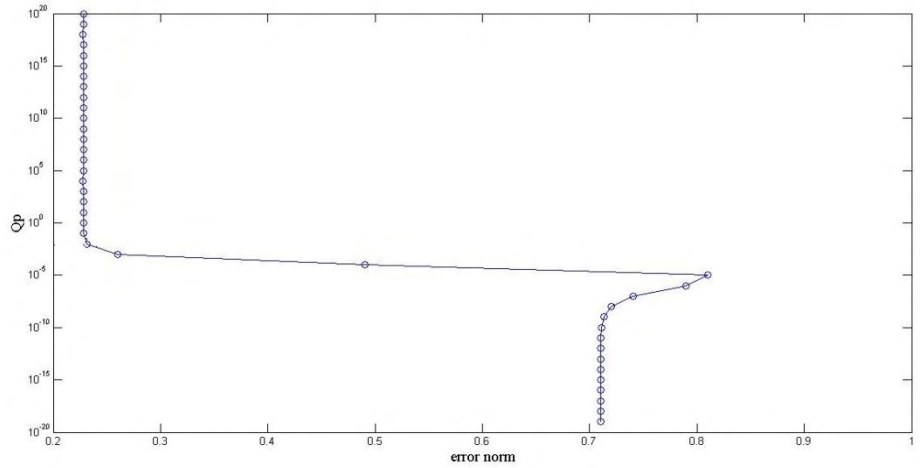

Figure 2.11: L-curve for the 2nd DOF.

Figure 2.11 shows that the acceleration MSE is steady until the input covariance matrix takes the crucial value Q^P= 0.01. For values between 0.01 and 0.00001 the MSE is increased rapidly. Until Q^P takes the value 10^{-10}, the MSE is downscaled and finally is steady when the $Q^P>10^{-10}$. As a result, one could choose for the particular example the crucial value Q^P=0.01. Consequently, the selected value for the input covariance matrix of the DOF2 is used in order to calculate the MSE and compare it with another value of the input covariance matrix.

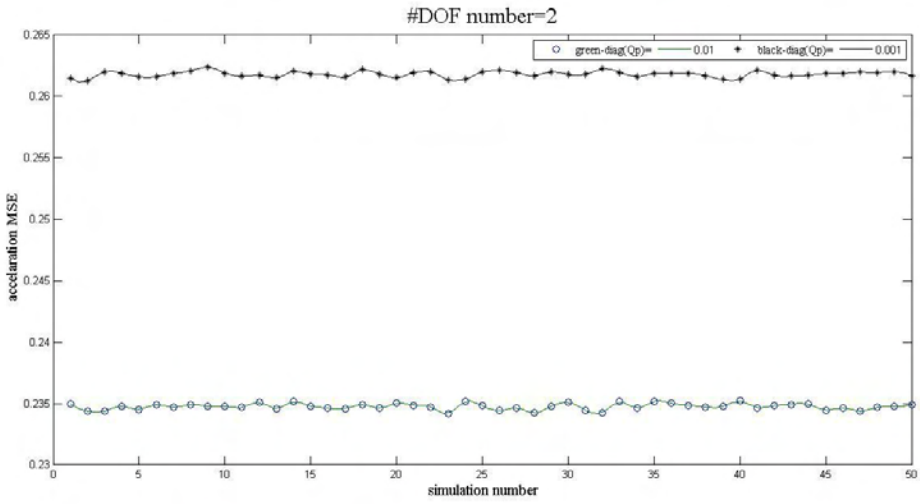

Figure 2.12: acceleration mean square error for the 2 DOF for Q^p=0.01 and Q^p=0.001, after 50 simulations.

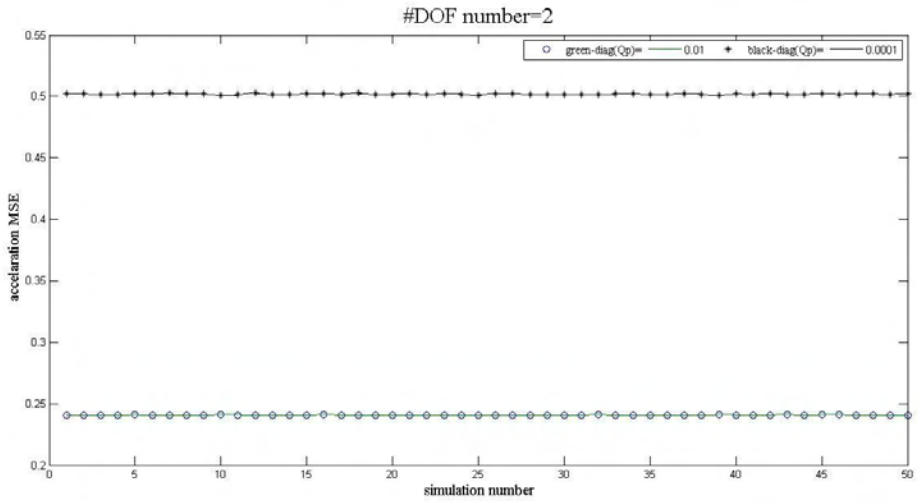

Figure 2.13: acceleration mean square error for the 2 DOF for $Q^{P=}0.01$ and $Q^{P=}0.0001$, after 50 simulations.

As we can see in figure 2.11 and figure 2.12, the L-curve provides an elegant initial estimation for the good-tuning of Q^P, because the acceleration MSE for DOF2 for $Q^P=0.01$ is better than the MSE for $Q^P=0.001$ and $Q^P=0.0001$. Furthermore, it is noted that there is an important improvement for the MSE, when the input covariance matrix takes the value of $Q^P=0.001$ than $Q^P=0.0001$. Notwithstanding, this improvement on the MSE is not as good as the improvement for $Q^P=0.01$. Thereupon the two values for the input covariance are used and results for the acceleration and displacement time histories are taken, in order to study the effects that Q^P has on the prediction of the acceleration and displacement by using Dual Kalman Filter. The model that it is used is the same as before and the diagonal components of R and Q^x are selected 0.0005 and 10^{-60} respectively. Measurements are taken from the 2 & 7 DOFS and the unknown force is applied on the 7 DOF.

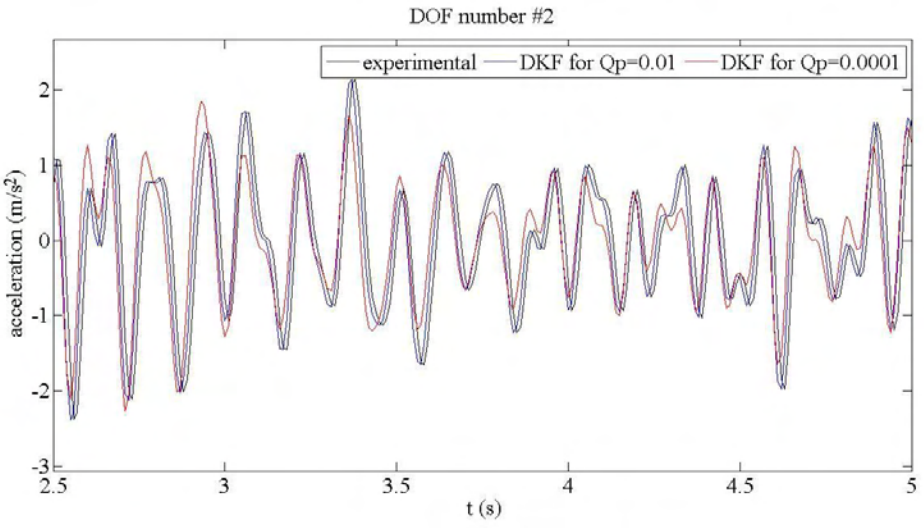

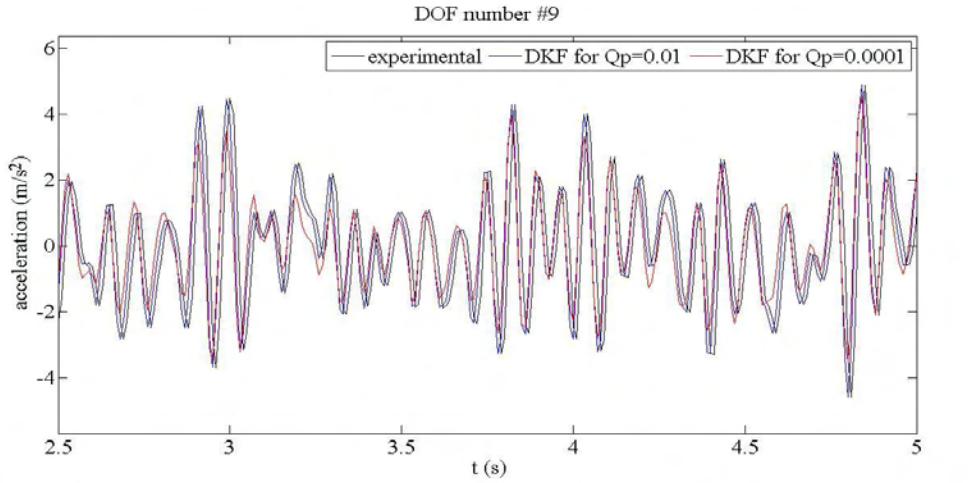

Figure 2.14: acceleration time histories for DOFS 2&9 from 2.5 to 5 seconds for Q^P=0.01 and Q^P=0.0001 by using Dual Kalman Filter.

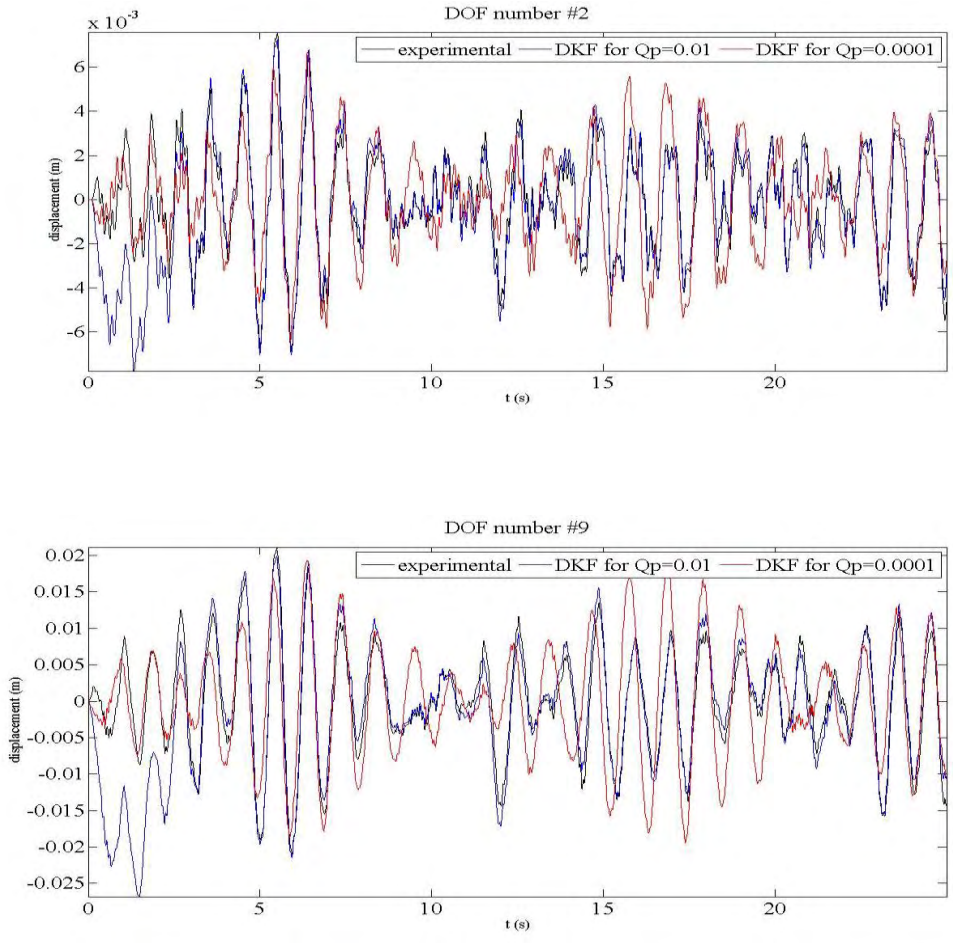

Figure 2.15: displacement time histories for DOFS 2&9 from 0 to 25 seconds for Q^P=0.01 and Q^P=0.0001 by using Dual Kalman Filter.

Comparing the results from the Figures 2.13 and 2.14, it becomes clear that the estimated acceleration and displacement time histories for input covariance Q^P=0.01 converge to its experimental time histories. On the contrary, one can see that for Q^P=0.0001 both time histories diverge off the acceleration and displacement experimental time histories that are calculated from the dynamics of the system. Note that, as it is shown in Figures 2.13 & 2.14, there are important issues like the so-called drift that affects the quality of acceleration and displacement estimates when the diagonal components of Q^P are set 0.0001. After the aforementioned study, one can come to the conclusion that Q^P= 0.01 is the best value for the input covariance matrix for the 10-DOF spring-mass chain like model that it is used in the analysis and as a result the L-curve can provide a suitable initial guess for the fine tuning of Q^p. Here, one can see that the values for the diagonal components of the covariance matrix of state that they were selected give a good predictions for acceleration and displacement time histories when the Q^P=0.01.

As it is shown in Figures 2.16 & 2.17 it is possible to take 100% accuracy for the acceleration predictions of the DOF where measurements are taken. Now the same 10-DOF model is used and the covariance of state is set 10^{-5}. Measurements are taken from the 2nd DOF.

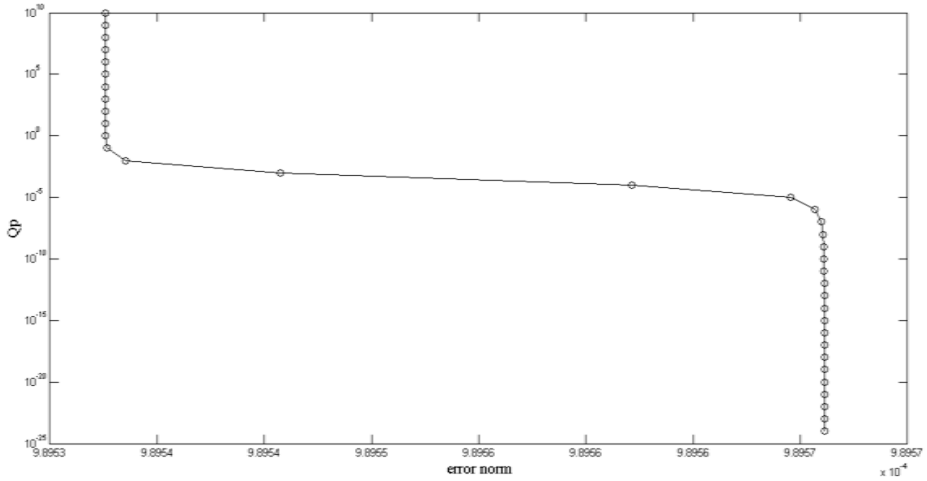

Figure 2.16: L-curve for the 2nd DOF.

From the Figure 2.16, one can easily observe that the error norm for Q^x=10^{-5} has decreased to 10^{-4}. This value is very small in respect off the error that it was taken in Figure 2.11 when Q^x was set 10^{-60}. Here, by studying the L-curve in Figure 2.16, the diagonal components of the covariance matrix of load is set 10^{-2}. The predictions that are taken for these values of the covariance matrix of state and load are presented in Figure 2.17

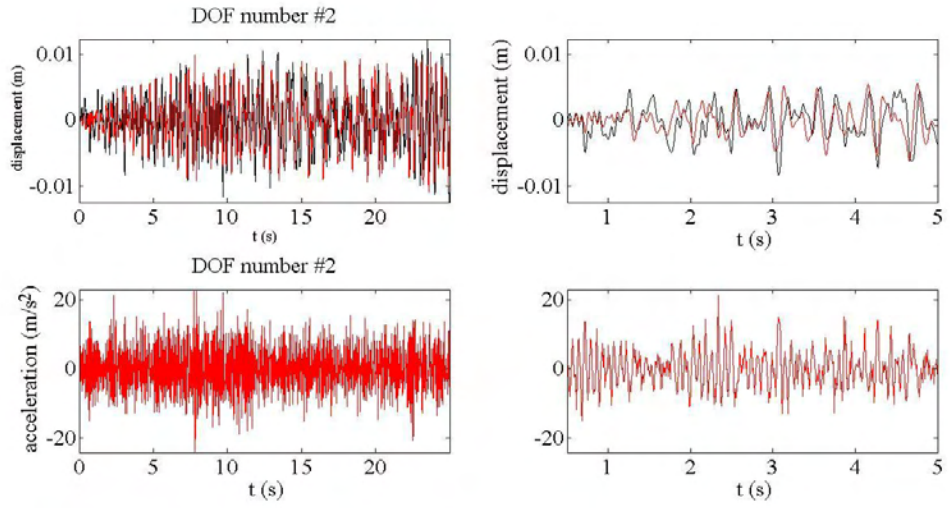

Figure 2.17: Acceleration and displacement time histories for the 2nd DOF. Comparison with the experimental time histories.

In Figure 2.17 it is seen that excellent predictions for the acceleration time histories are taken when the diagonal components of the matrices Q^x and Q^P are set 10^{-5} and 10^{-2} respectively. On the contrary, the predictions for the displacement time histories are worse from the predictions that were taken in Figure 2.15.

Generally the L-curve is used in order to take excellent acceleration predictions. On the contrary, as it is shown above it is possible to take very bad predictions for the displacement time histories when 100% accuracy in acceleration predictions are taken. The best way to take very good predictions for both acceleration and displacement is to choose a value near the best optimal value that someone finds with L-curve. Also it is very important to choose carefully the diagonal components of the covariance matrix of state because it affects the predictions as it was seen above.

2.8 Tuning the observation noise covariance matrix

In the last section of this chapter the L-curve is studied in order to estimate the appropriate diagonal components of the Q^P. Now, a methodology is discussed in order to tune the observation noise matrix R. For this, the acceleration measurements time histories are used. Also the standard deviation of each acceleration measurement $y_{ini}=\sqrt{\frac{\sum_{k=1}^{N} d_k^2}{N}}$ is introduced, where N is the number of values of each measurement and d_k are the acceleration measurements. Furthermore it is assumed that the standard deviation is approximately 1.25% of acceleration peak for each measurement. For the measurements in this example it is decided that $s=\frac{1}{100}\, y_{ini}$. Finally, the observation error covariance is estimated from the equation $R=s^2 I$, where I is an identity matrix with appropriate dimensions. In this example the acceleration measurements peaks are near to 5 m/sec^2. As a result, for the first measurement $s_1=0.03$ and for the second measurement $s_2=0.05$ where $s=\begin{bmatrix} s_1 \\ s_2 \end{bmatrix}$.

CHAPTER 3 Robust Response Prediction in the Spring-Mass Chain- Like Model

3.1 Introduction

In the analysis herein, an attempt is made to consider the uncertainties when the precise values of the stiffness are unknown. Conversely, the mean and the standard deviation of the uncertainties are known, making the assumption that the stiffness follow a Gaussian distribution, such as $k_i = k_0(1+e_i)$, where $e_i \sim N(m, s_i^2)$, k_i is the stiffness values for each spring, where index i is the number of the spring. The objective in this part is to demonstrate the simulations and the results for the robust response prediction of the acceleration and displacement time histories and also to display the boundaries for the acceleration and displacement that arise from the quantiles of the samples.

3.2 Simulated example

Hence the 10 DOF spring-mass chain-like model is used. In this section, it is assumed that the stiffness follows a Gaussian distribution with mean=650 *N/m* and s_i=0.1*mean and the uncertainties are inserted in the first and the fifth degree of freedom. The number of the samples of the uncertainties which are produced from the Gaussian distribution is 20 and herein two samples are selected for demonstration. Measurements are taken from the second and the seventh DOF. The unknown input force is applied to DOF 7. The diagonal components of the covariances Q^P, Q^x, R could be set to 0.02, 10^{-40} and 0.001 respectively. It is assumed that Q^P and Q^x are equal to the initial values of the covariance of input and state.

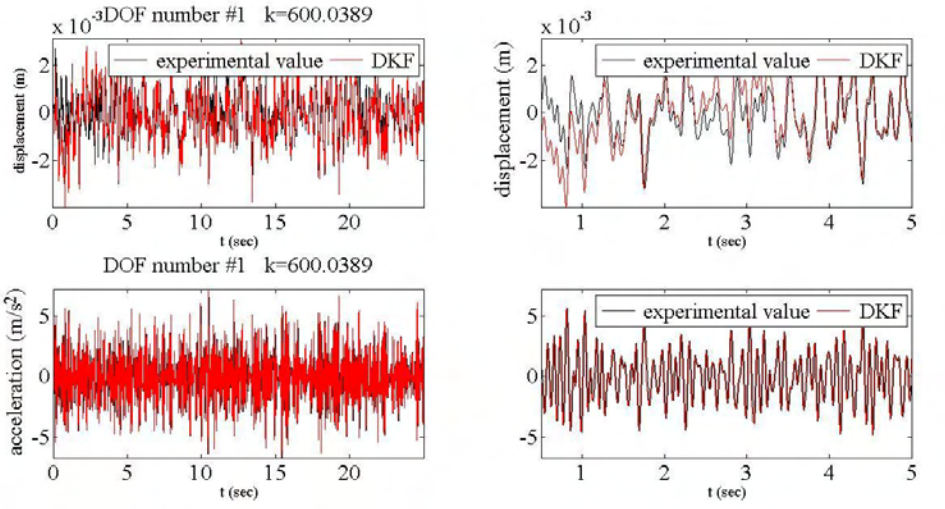

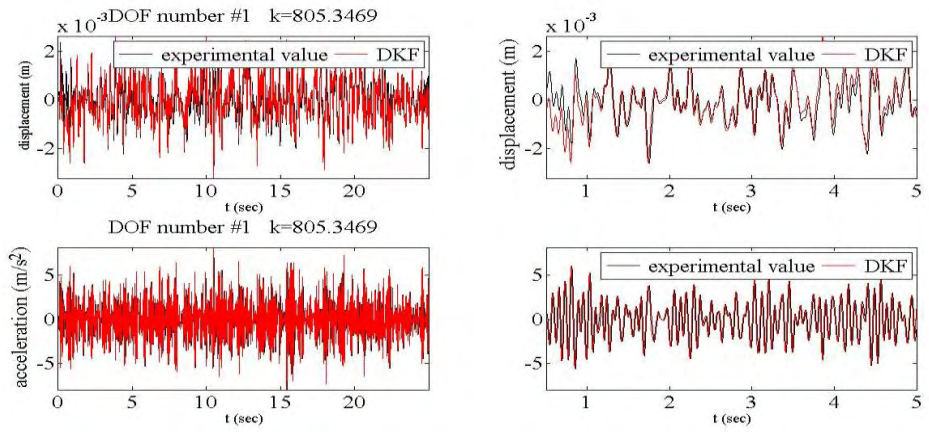

Figure 3.1: Acceleration and displacement time histories estimated by the Dual Kalman Filter at DOF 1, using two samples.

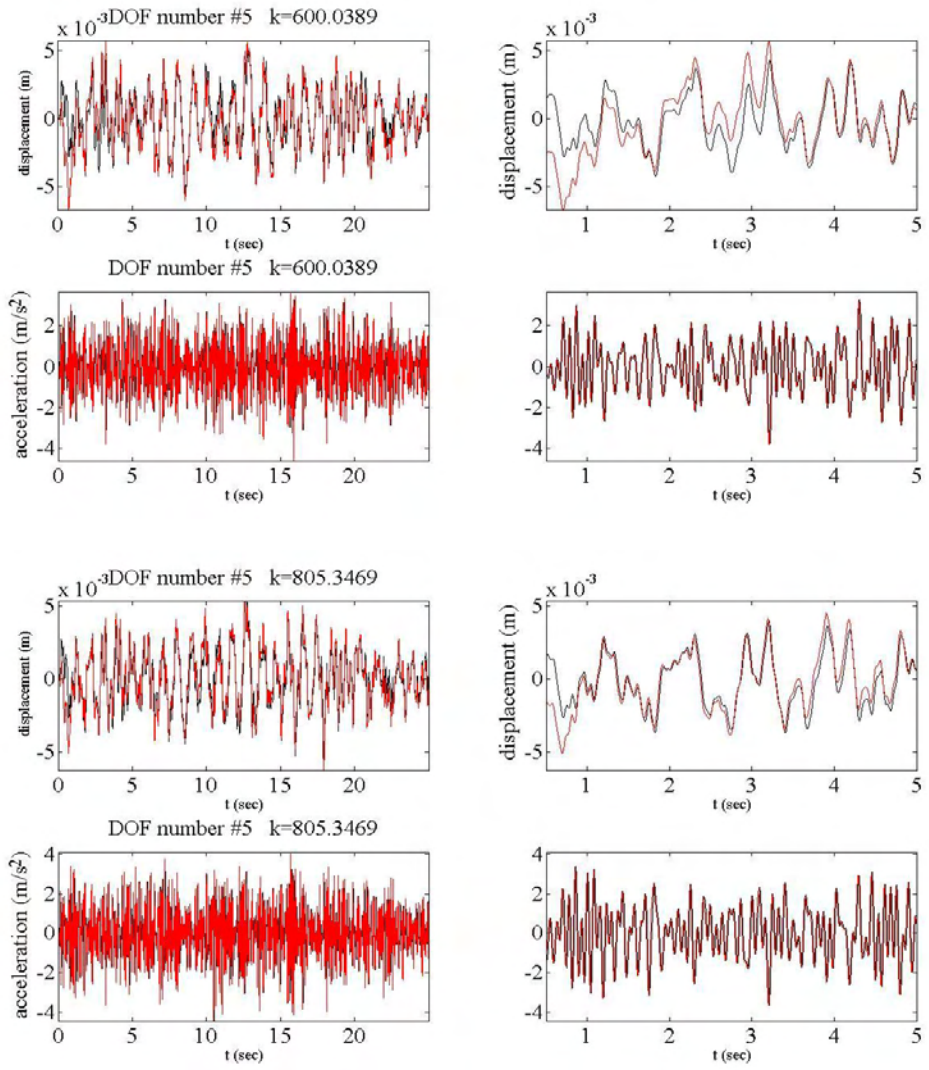

Figure 3.2: Acceleration and displacement time histories estimated by the Dual Kalman Filter at DOF 5, using two samples.

In Figure 3.1 and 3.2, time histories at DOF 1 and 5 are estimated by using acceleration measurements from the DOF 2 and 7. It is observable, that the prediction of acceleration time histories is very accurate. On the contrary, the predicted displacement time histories diverge from the experimental displacement time histories for the same DOF, mainly at the first two seconds of the simulation. As time goes by, the deviations are minimized. That drift is happening, because the value of Q^P, Q^x and R must be chosen carefully so that highly accurate predictions could be done. This problem is studied in different section.

Furthermore in Figures 3.3 – 3.5 the acceleration, displacement and force prediction for the 1st DOF of the system for three stiffness uncertainties are presented. Note that the stiffness of the 7st and 8th spring has a constant value of 650 N/m. The objective in this part is to find if the uncertainties in the 1rd and 5th spring affect the predictions of the 7th DOF.

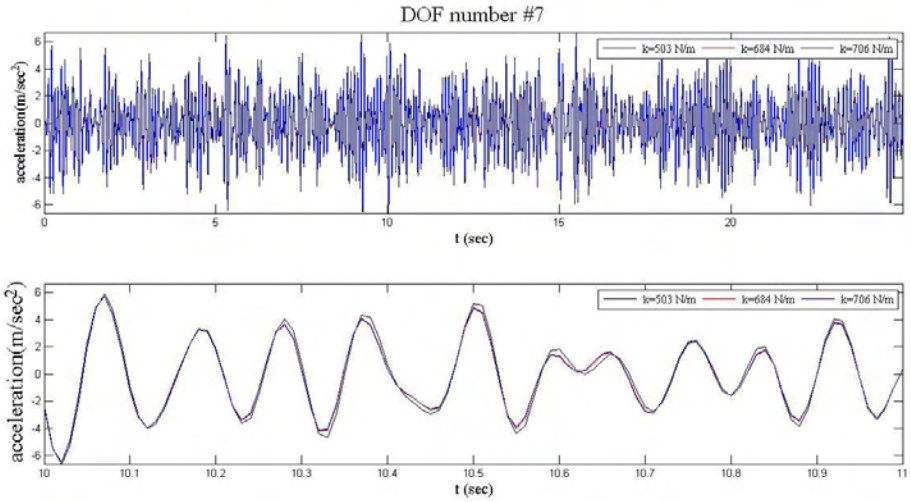

Figure 3.3: Acceleration time history estimated by the Dual Kalman Filter at DOF 7, using three samples.

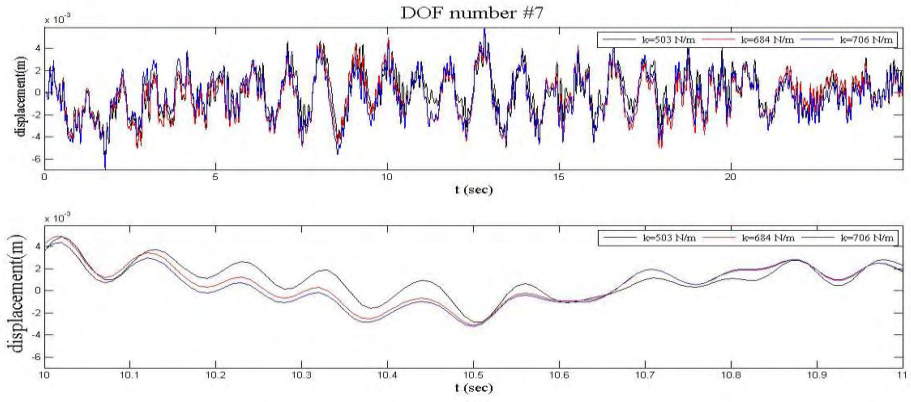

Figure 3.4: Displacement time history estimated by the Dual Kalman Filter at DOF 7, using three samples.

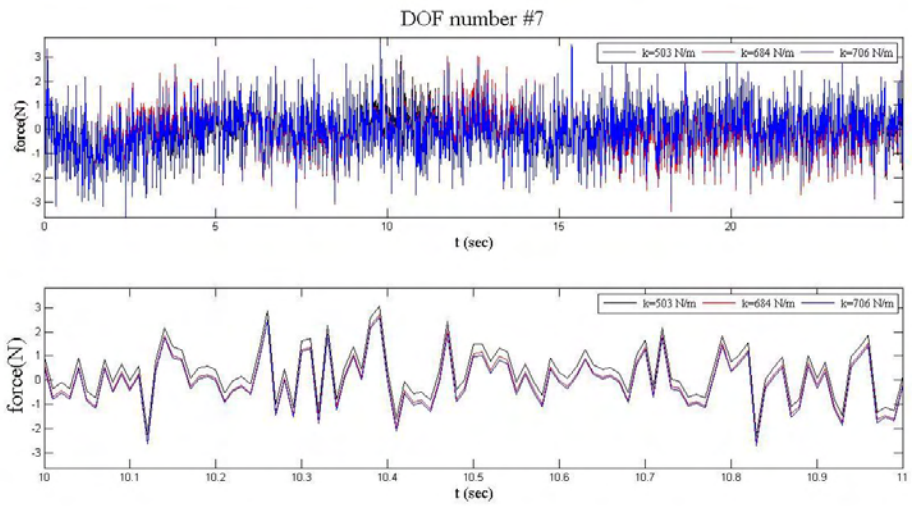

Figure 3.5: Force time history estimated by the Dual Kalman Filter at DOF 7, using three samples.

In Figure 3.3, 3.4 & 3.5 it can be observed that for the 7th DOF where the 7th and 8th spring's stiffness has constant value the prediction divergences for the acceleration, displacement and force prediction for three stiffness cases are small. The biggest divergences are observed in the displacement time histories. In the acceleration and force time histories the divergences are almost zero. It is safe to extrapolate that the uncertainties in some springs are crucial mainly for the prediction of the displacement time histories and affect all the system.

3.3 Boundaries by using quartile theory

For each point of the 2500 that are used for the simulation, the samples for acceleration or displacement prediction time histories are used in order to estimate the uncertainty as a function of time. By applying the quartile theory, the samples' Gaussian distribution is divided into four groups with equal probabilities. By applying this theory, we were able to find the upper, mean and lower quartile for each data point, by combining all the samples of

the uncertainty. As a result, three curves in time are taken, one for each quartile.

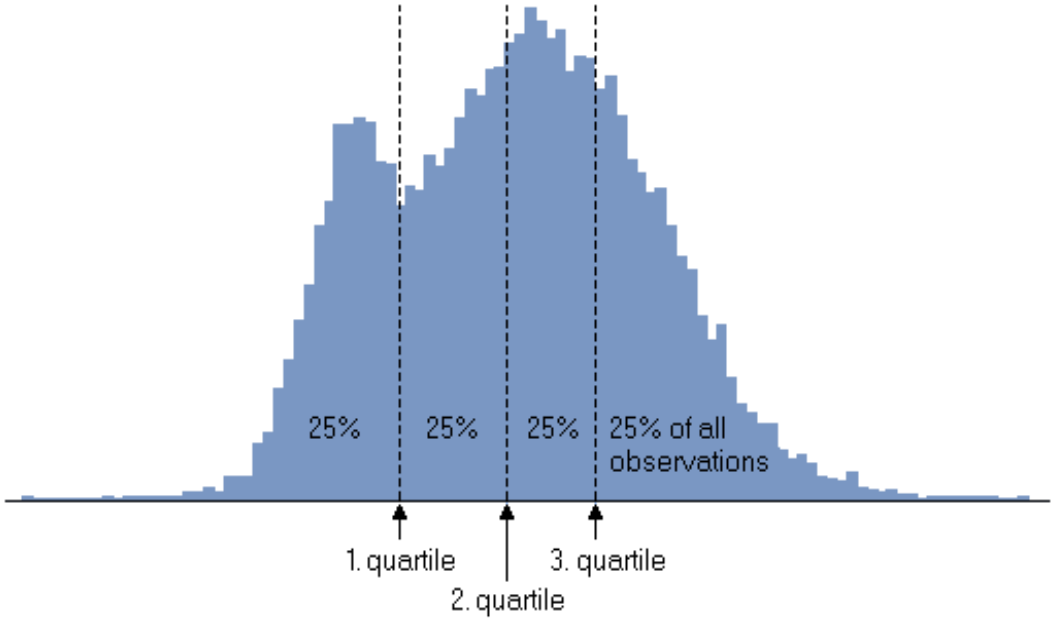

Figure 3.6: quartiles application in a Gaussian distribution.

This procedure is demonstrated for acceleration, displacement and force time histories and it is used to place boundaries in the experimental value. The DKF procedure is used here. It is assumed that stiffness uncertainties are inserted in the 5th spring. The uncertainties are produced from a Gaussian distribution with mean=650 *N/m* and standard deviation s=0.1*mean. The samples of the uncertainties are 100. These samples are used in order to calculate the quartiles of the 5th spring. The 5% 50% and 95% quartile prediction bounds of the acceleration and displacement prediction time histories are shown in Figures 3.7 – 3.9.

a

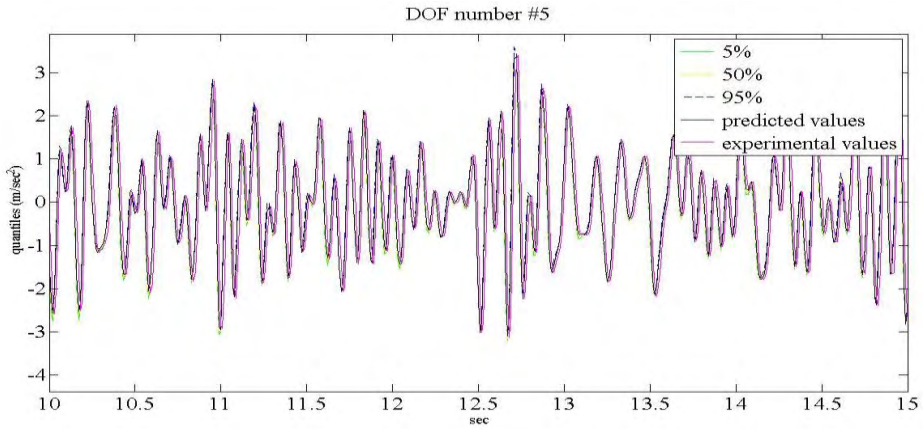

b

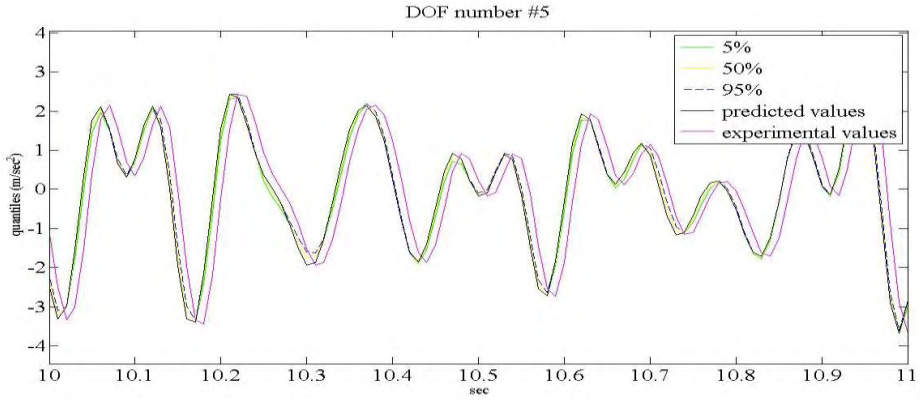

Figure 3.7: (a) Complete and (b) detail acceleration boundaries and experimental acceleration time history for DOF 5.

a

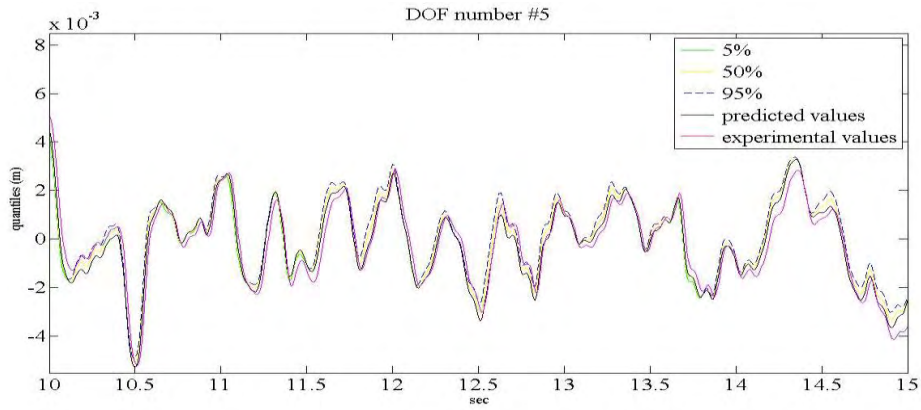

b

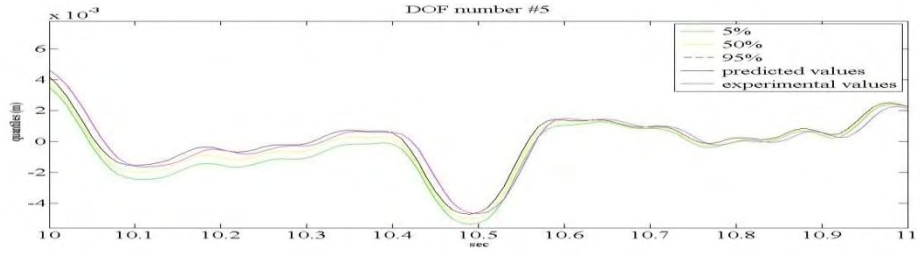

Figure 3.8: (a) Complete and (b) detail displacement boundaries and experimental displacement time history for DOF 5.

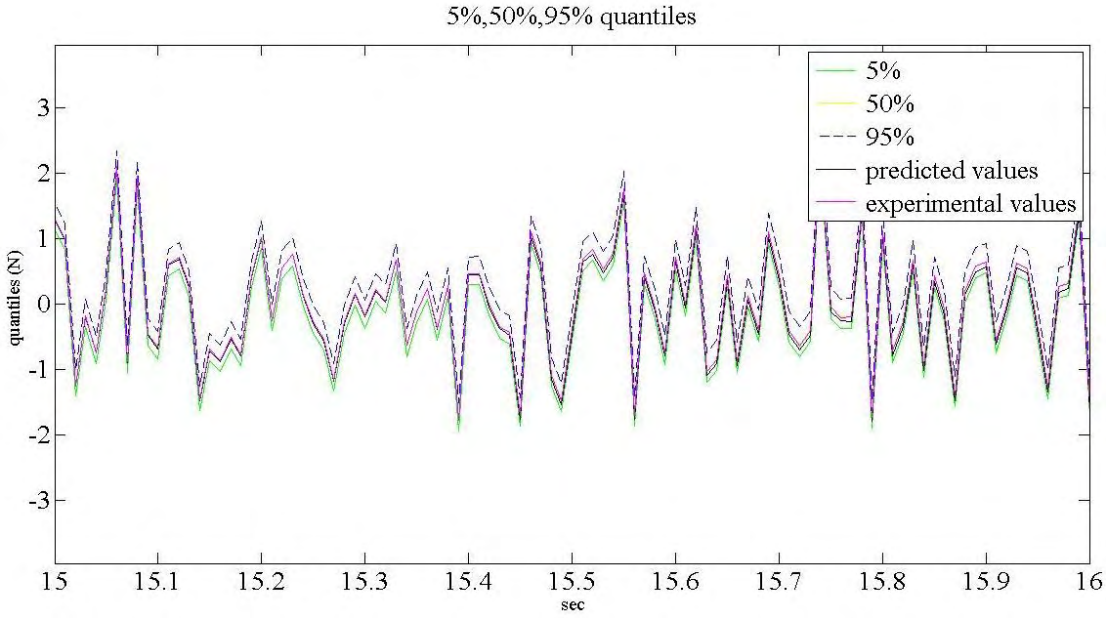

Figure 3.9: 5%, 50%, 95% quartiles of the predicted time histories and the experimental force time history for 15-16 sec.

It can be seen in Figure 3.7 and 3.8, that there are some points where the experimental acceleration or the displacement excitation exceeds the 5% and 95% bounds. Generally, one can say that the experimental time histories are inside the boundaries of 5% and 95% and they almost coincide with the predicted acceleration and displacement time histories. Also in Figure 3.9 one can see that the experimental and predicted force time histories are inside the boundaries which are defined form the quartile theory. It must be noted the fact that the difference between the upper and the lower quartile as the time pass is minimized.

3.4 Conclusion

In this section the uncertainties in the stiffness of the 10 DOF spring-mass chain-like model are considered. At the first part of this section simulated examples for two DOFS of the system are presented. It can be seen that the uncertainties of each spring affect the acceleration and displacement response of the two adjacent degrees of freedom. According to the final conclusions, it is easy to tell that the uncertainties in a system play a crucial role for the safety of the system and structure. Secondly, it is shown that by applying the quartile theory for the predicted acceleration and displacement time histories it is convenient to put boundaries for the experimental time histories. Furthermore, one can conclude that the experimental responses for acceleration, displacement and force are inside the 5% and 95% quartile, except some occasions. It is safe to tell that the noise that is added in the Dual Kalman Filter is responsible for these occasions. If the tuning of the noise covariances matrices is badly scaled, then the experimental acceleration and displacement time histories will exceeds the boundaries that are set from the 5% & 95 quartiles.

Chapter 4 Prediction of Fatigue Damage Accumulation in Metallic Structures

4.1 Introduction

In this section, a fatigue lifetime prognosis of a metallic structure under uncertainties is taken place. Assume that there is a metallic structure that is subjected to varying load events and let $f_i(t)$ be the excitation time history for the load event i. Furthermore, let d_i be the fatigue damage due to i-th load event. In order to make the fatigue lifetime prognosis at any point of the structure, a dual Kalman filter is used in order to predict strain and stress time histories where measurements are not available. For example, it is impossible to install sensors to underwater structures. Specifically, taking output-only measurements from a limited number of measured locations, one can use the aforementioned dual Kalman filter to predict the stress at all hotspots locations, without knowing the distribution of the load applied on the structure. It is well known that, in such systems uncertainties are involved. For example, one could introduce uncertainties in the parameters involved in the S-N models, the prediction error from these models and finally, in the model associated with the linear damage accumulation rule. These types of uncertainties and their effects on the fatigue damage accumulation will be studied herein. The objective of this chapter is to calculate the remaining fatigue life at every location of a spring-mass chain-like model. For this purpose the distribution of the load and the structural and fatigue model parameters are given. Also the effects of the uncertainties on the fatigue damage accumulation and lifetime is studied and discussed herein.

4.2 Stresses and fatigue damage-general methodology

As it is said above, to calculate the fatigue damage accumulation in a metallic structure, one has to use the stress time histories which are obtained by the dual Kalman Filter procedure. Once the stress time histories are calculated for all the hotspots of the metallic structure, fatigue damage accumulation models will be used, to estimate the fatigue and the remaining life at all points or at some points (hotspots) of the system. Note that, a Rainflow stress cycle counting methods are also used for the fatigue prediction. To predict and estimate d_i, one has to use the Palmgren-Miner rule (Plamgren1924, Miner 1945). Defining, **k** as the future events, **D** the linear damage accumulation, $\mathbf{n_i}$ is the number of cycles at a stress level $\mathbf{s_i}$ and $\mathbf{N_i}$ is the number of cycles required for failure at a stress level s_i, the damage accumulation D at a point in the structure is given by

$$\mathbf{D}=\sum_{i=1}^{k}\frac{\mathbf{n_i}}{\mathbf{N_i}} \qquad \mathbf{(1)}$$

Damage occurs when D=1. Alternative, the structure is safe when $\sum_{i=1}^{k} d_i$<1

Moreover, in order to calculate the number of cycles required for failure, the S-N fatigue curves are adopted. The curves are obtained from laboratory experiments on simple specimens that are subjects to constant loads. Recombining them with stress cycle counting

method, such as the Rainflow cycle-counting method, the number of cycles n_i at a stress level s_i is determined. Next, the Goodman relationship is defined, in order to determine the modified stress cycle range

$$\Delta s_{Rt} = \Delta s_R \left(1 - \frac{s_m}{s_u}\right) \qquad (2)$$

where Δs_R is the stress cycle range, s_m is the mean stress and s_u is the static strength of the material. Recombining the equations (1) and (2), the following rule for the estimation of the fatigue damage is estimated:

$$D = \sum_{i=1}^{k_1} \frac{n_i}{N_f} \frac{\Delta s_i^{\,m}}{\Delta s_D^{\,m}} + \sum_{j=1}^{k_2} \frac{n_j}{N_f} \frac{\Delta s_j^{\,m+2}}{\Delta s_D^{\,m+2}}$$

The first term of the rule above applies for $\Delta s_i \geq \Delta s_D$ and the second term applies for $\Delta s_L \leq \Delta s_j \leq \Delta s_D$. N_i and n_j correspond to the number of cycles in each stress range respectively, Δs_i and Δs_j are the ith and jth stress ranges, k_1 and k_2 are the number of the different stress range blocks above or below the constant amplitude fatigue limit Δs_D. Finally, Δs_D and Δs_L is the constant amplitude fatigue limit and the cut-off limit respectively. According to the Eurocode for detail category 36, m, Δs_D and Δs_L are defined 3, 26.5 and 14.5 respectively.

4.3 Fatigue damage accumulation without uncertainties

In Figure 4.1 is presented the fatigue damage accumulation for a 20 DOF spring-mass chain-like system, using stresses which are calculated from the data predicted by the DKF's simulations and stresses from the experimental time histories. For the dual Kalman filter prediction, it is assumed that k=650 *N/m* and m=0.35 *kg*. Acceleration measurements for the dual Kalman filter are taken from the 3 & 7 DOF and the force is applied on the 7 DOF. The diagonal components of the covariance matrices Q^P, Q^x, R are selected 10^{-3}, 10^{-27}, 0.003 respectively. Furthermore it is assumed that there is no uncertainty in the model and that $k_1=k_2=\ldots=k_{20}=650$ *N/m*.

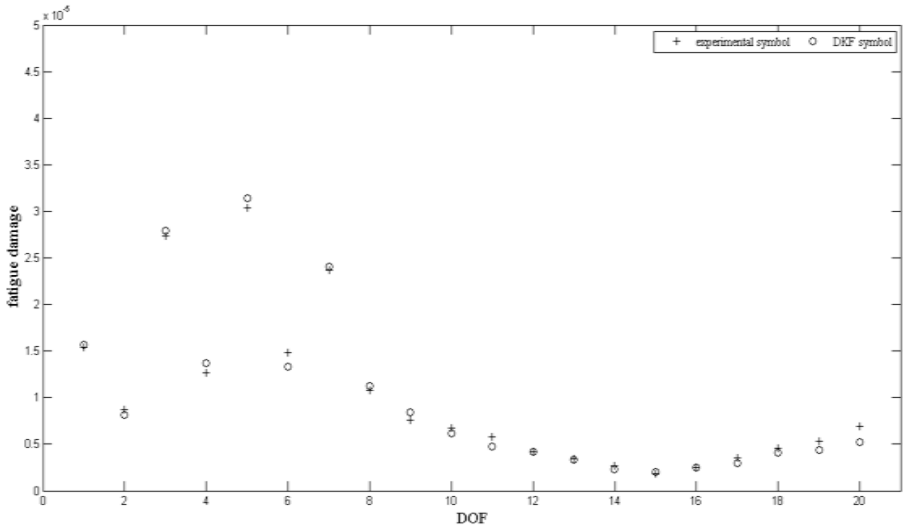

Figure 4.1: Fatigue damage accumulation of the 20 DOF spring-mass chain-like model.

It can be seen in Figure 4.1 that the 3, 5 and 7 springs suffer the most from fatigue damage and these are the three crucial hotspots of the system. It seems that most of the damage is around the area where the force is applied. It is remind that the force is applied to the 7^{th} DOF. The springs which are further from the area of force are the safest. Note that the estimation's accuracy of the fatigue damage is very high and that means that the algorithm for estimation the fatigue damage accumulation is a valuable tool for designing optimal fatigue-based maintenance strategies in a wide variety of structures.

4.4 Robust Fatigue Damage Accumulation

The objective in this part is to examine and study how the fatigue damage in a 10-DOF spring-mass chain-like model is affected, when the uncertainties of the model is taken into account. Uncertainties in this problem arise from the fact that we don't know precise the values of the stiffness, mass or the damping matrix of the model. It is assumed that uncertainties are imported in the 1^{st} and 4^{th} springs of the system. Let k_i be the stiffness values for each spring, where index i is the number of the spring. Also, it is assumed that k_i have the following form: $\mathbf{k_i=k_{0,i}(1+e_i)}$, where $k_{0,i}$ are the nominal values used in DKF algorithm, and that e_i are the samples of the uncertainties that follow a Gaussian distribution, such that $e_i \sim N(k_{0,i}, s^2)$. Hence, for the sake of simplicity, assume that $k_{0,1}=\ldots. =k_{0,ndof}=k_0=650$ *N/m*. Combining this procedure with the general methodology of the fatigue damage that is shown above, we run simulations at any degree-of-freedom of our system. By using acceleration measurements from a limited number of locations in the structure, one can estimate the fatigue damage accumulation d_i at different points or at all locations. Hence, we must point that first we use the displacement time histories from the DKF in order to estimate the stresses at any location of the system. These stress time histories are used in the fatigue algorithm, to find the damage values and the fatigue lifetime anywhere in the system. In addition, the values of the d_i are used to obtain an estimate of the PDF, $p(d_i)$.

In Figures 4.2-4.5, histograms of fatigue estimations are shown from DKF simulations. It is assumed that all fatigue histograms follow Gaussian distribution. Two springs are chosen randomly and their pdf are presented herein. For the first two PDFs 200 samples drawn from an assumed normal distribution with mean=k_0=650 *N/m* and standard deviation=s=0.1*k_0. The spring mass chain system is made of steel, and each spring has length L_0=0.3, tensile modulus $2.1*10^3$. To estimate the stress time histories everywhere in the system, the equation $k_i=\frac{E_i A_i}{L_0}$ is used in order to find the A_i for each spring. It can be shown that the $p(d_i)$ for the selected springs of the system follow a Gaussian distribution.

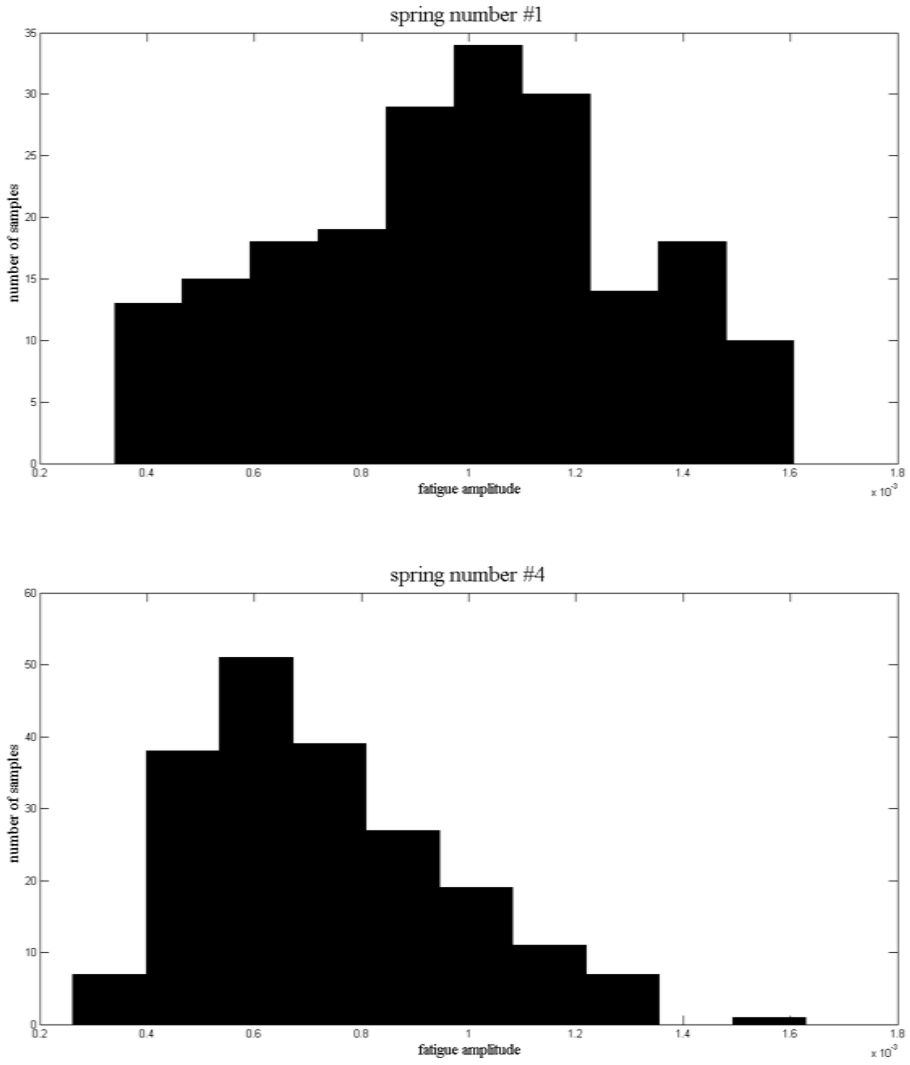

Figure 4.2: Histograms of fatigue estimates (200 samples) with $s=0.0001*k_0$

For the second two PDFs 850 samples drawn from an assumed normal distribution with mean=k_0=650 and standard deviation=$s=0.1*k_0$.

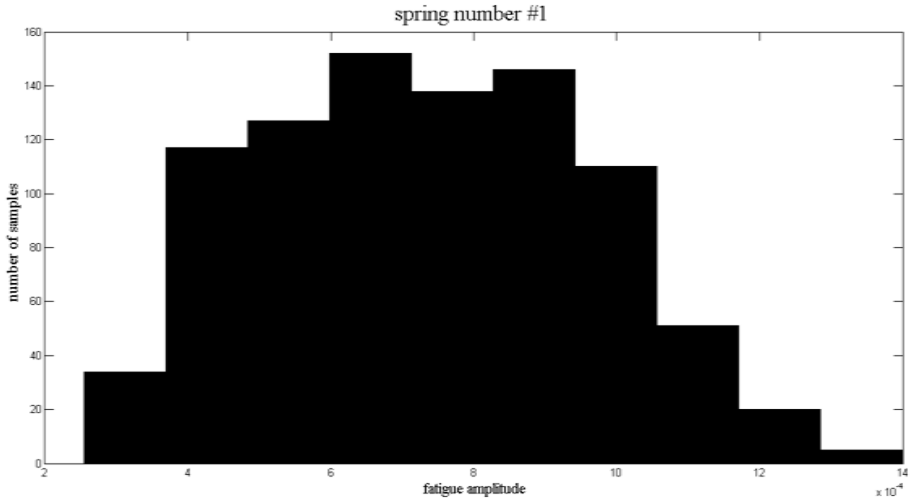

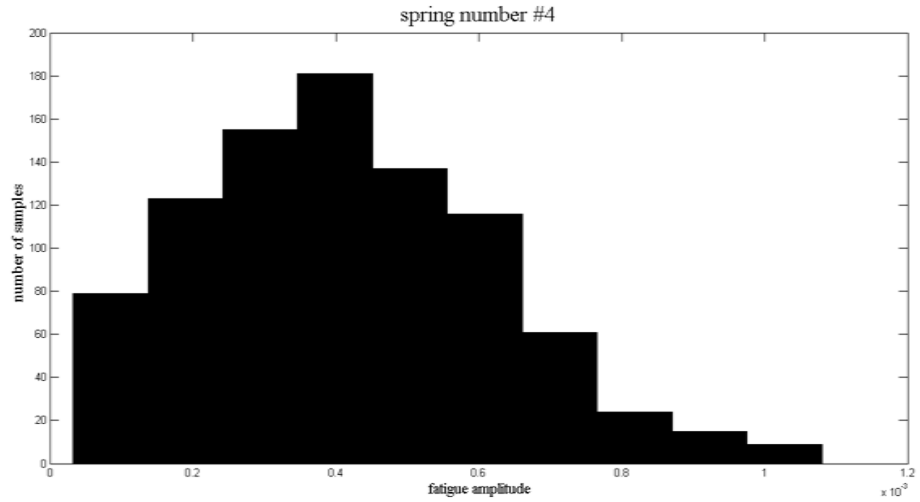

Figure 4.3: Histograms of fatigue estimates (900 samples) with s=0. 1*k_0

Furthermore, if the standard deviation of the uncertainties is changed, the results for a certain spring is shown.

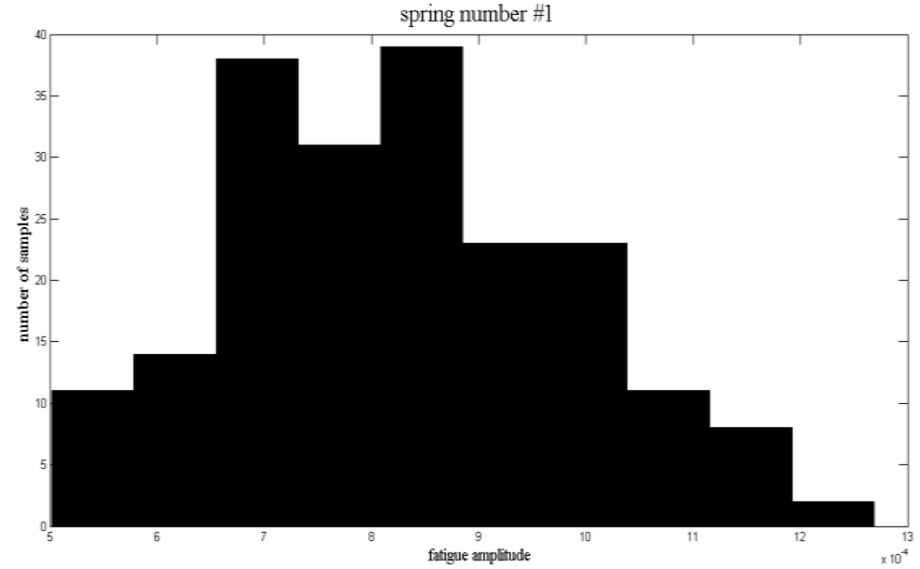

Figure 4.4: Histograms of fatigue estimates (200 samples) for the 1st spring, with s=0.0001*k_0

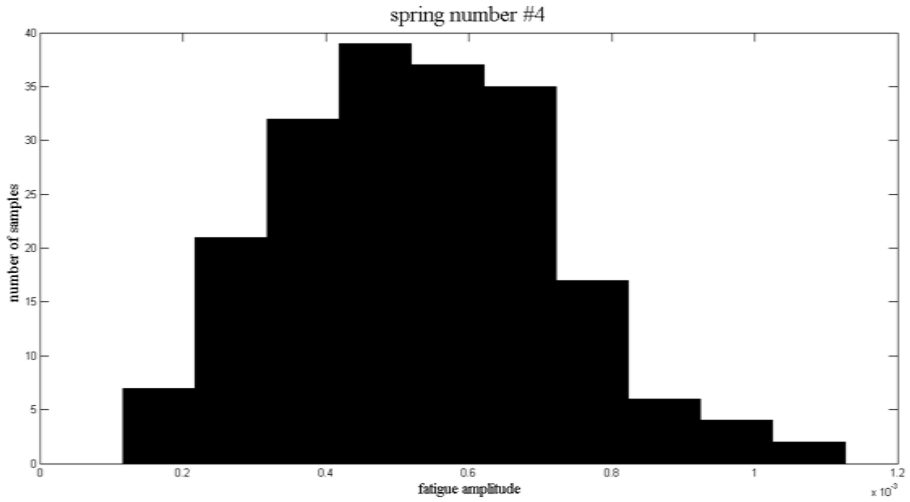

Figure 4.5: Histograms of fatigue estimates (200 samples) for the 4st spring, with s=0.0001*k_0

Note that when the standard deviation of the samples is diminished, the amplitude of the fatigue is reduced. From the Figures 4.2, 4.3, 4.4 and 4.5 can be seen that the fatigue damage curve seems like a Gaussian distribution when the uncertainty is produced from a Gaussian distribution. Moreover, could be shown that when the number of samples is increased, the fatigue histograms seem better like a Gaussian distribution.

The aforementioned analysis can be used to calculate the fatigue damage accumulation and the fatigue lifetime everywhere in the 10 DOF chain-like model. It is assumed that uncertainties are inserted in the 1st , 3rd, 5th,7th and 9th spring and the force is applied on the 3 DOF of the model. We choose 2 samples for the 1, 3, 5, 7, 9 springs, with k=mean=1000 *N/m* and s=0.1*mean. The results are computed and reported in Table 4.1.

Number of spring	Sample	Fatigue accumulation	Fatigue lifetime (days)
1	1000	0.0022	12.9153
	1100	0.0021	134725
3	1000	0.0032	**9.1202**
	1100	0.0034	**8.5101**
5	1000	0.000971	29.7859
	1100	0.000835	34.6409
7	1000	0.000851	34.0036
	1100	0.000638	45.3096
9	1000	0.000486	59.5283
	1100	0.000988	29.2820

Table 4.1: Fatigue accumulation and fatigue lifetime for two samples of the stiffness, for 5 springs.

It can be seen that damage due to fatigue will occur first at the third spring, and then at the first spring. It seems logical because the force is applied to the 3rd DOF of the model. Also, it is reminded that the aforementioned analysis can be used at every point in the structure. The lasts springs of the system seems to be the safest, because the fatigue lifetime is bigger in these springs.

In the last part of this section the possible effects that stiffness uncertainties have on the fatigue damage accumulation of a spring are studied. It is assumed that a 10-DOF spring-mass chain like model is used and stiffness uncertainties are introduced only in the 4th spring. The uncertainties follow a Gaussian distribution with mean=650 *N/m* and standard deviation s=0.1*mean. It is chosen that the samples of the uncertainties are 100. All the other springs of the system have stiffness k=650 *N/m*. The force is applied on the 4 DOF and the acceleration measurements are taken from the 4 DOF. In the following two figures the stiffness samples and the fatigue damage for its sample are presented for the 4th spring.

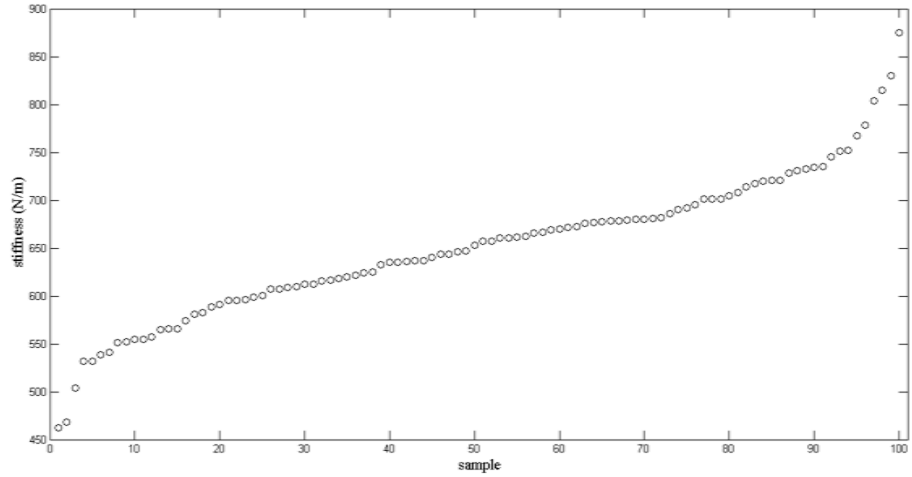

Figure 4.6: the stiffness samples which are produced from a Gaussian distribution.

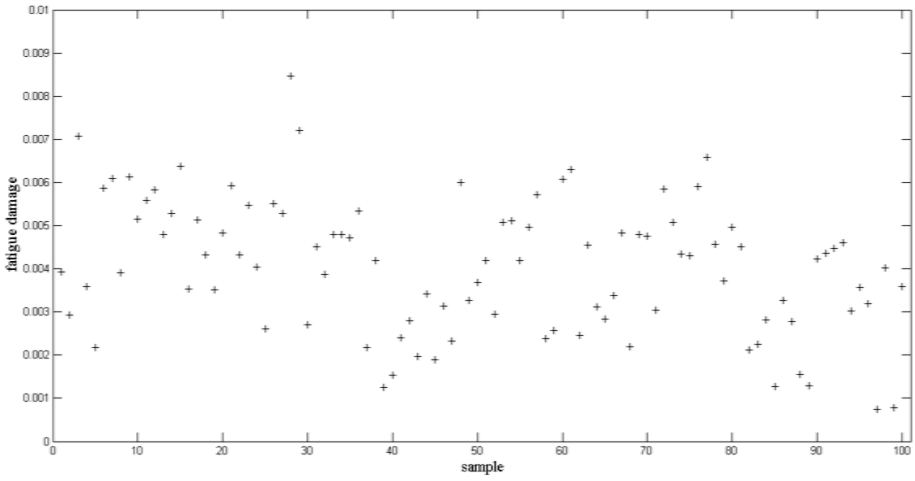

Figure 4.7: fatigue damage accumulation for each stiffness sample.

By seeing the Figure 4.6 and Figure 4.7 it is safe to conclude that the fatigue damage accumulation for a particular spring does not follow the increased trend of the stiffness uncertainties. On the contrary it seems that there is a random distribution in the fatigue damage accumulation.

In the last part of this section it is assumed that a 10-DOF spring-mass chain like model is used. It is assumed that acceleration measurements are taken from the 3rd and 7th DOF. Force is applied on the 3rd and 7th DOF. Additionally we choose to insert uncertainties to all the springs of the system. The uncertainties follow a Gaussian distribution with mean=650 *N/m* and standard deviation s=0.1*mean. The samples of the uncertainties are 300. In order to find an average for the fatigue damage accumulation for all the samples and spring, the following equation is used: **fatigue for a spring=**$\int_{\mathbf{i=1}}^{\mathbf{300}} \mathbf{fatigue_i/300,}$ where samples=300**.** The results for the fatigue damage accumulation and lifetime prognosis are presented in the following table.

Spring number	Average of fatigue damage accumulation	Average of lifetime Prognosis
1	0.00365	**9.6736**
2	0.0022	26.5625
3	0.0036	**10.9557**
4	0.00322	**12.2244**
5	0.0032	12.9669
6	0.0025	23.8965
7	0.0029	19.2125
8	0.0012	40.5083
9	0.0018	31.7525
10	0.0031	17.4712

Table 4.2: Average of fatigue damage accumulation and lifetime for all the springs of the system when there are uncertainties.

It can be seen in Table 4.2 that the first three most damaged springs are the 1st, 3rd and 4th spring. On the contrary the safest springs are the 8th, 9th and 2nd spring. With this methodology one can easily predict the fatigue damage accumulation and lifetime all over the metallic structure when the stiffness of the springs is not known and we know only the mean and the standard deviation of the stiffness.

4.5 Conclusion

The study of the aforementioned chapter was focused on the calculation of the fatigue damage accumulation for a linear N-DOF spring-mass chain-like model. Firstly, in section 4.2 the basic mathematical relationships were presented and a method was proposed in order to calculate the fatigue damage accumulation in a linear model using stress time histories for all over the structure. In section 4.3 a 20-DOF spring-mass chain like model was used and the fatigue damage for all the springs of the model was calculated. Finally, in section 4.4 uncertainties of the stiffness were taken into account and simulations were done in order to study how the uncertainties affect the fatigue damage of the system. It was seen that damage is greater in the area where the force is taken place. It becomes clear that the uncertainties of the springs are crucial for the study of the fatigue damage of a linear system.

Chapter 5 Robust Sensor Optimization Placement

5.1 Introduction

In this section, a method is presented to determine the optimal sensor placement in the linear system which was used in the previous chapters. Additionally, the effects of the uncertainties associated with stiffness and the errors on the sensor's optimal placements are investigated. The uncertainties follow a Gaussian distribution with $e_i \sim N(m,s^2_i)$ and covariance Q. Herein, by assuming the aforementioned second order linear structural dynamics problem, the sensor location that minimizes the trace and the determinant of the state error covariance is determined. It will be shown that, by solving the Ricatti equation for $\dot{P}=0$, we are able to find the optimal sensor placement for the linear problem.

5.1.1. Mathematical approach

By following the work of Eric M. Hernandez [21], we propose the following methodology. The first step is to introduce the state error covariance matrix, which is estimated by the Ricatti equation

$$\dot{\mathbf{P}}(t) = \mathbf{AP}(t) + \mathbf{P}(t)\mathbf{A}^T - \mathbf{K}(t)\mathbf{R}(t)\mathbf{K}(t)^T + \mathbf{Q}(t) \quad (1)$$

where K(t) is the Kalman gain of the state estimate $\hat{x}(t)$ and

$K(t) = P(t)C^T R(t)^{-1}$

Furthermore, the covariance matrices $Q^P=Q_0$ and $R=R_0$ are reminded. By applying the aforementioned Ricatti equation, the equation (1) is solved for $\dot{P}=0$ and for steady-state condition $P=P_s$.

$$\mathbf{0} = \mathbf{AP_s} + \mathbf{P_s}\mathbf{A}^T - \mathbf{P_s}\mathbf{C}^T\mathbf{R_0}^{-1}\mathbf{C}^T\mathbf{P_s} + \mathbf{Q_0} \quad (2)$$

where **A,C** are the system matrices from the state-space equation in continuous time and $\mathbf{R_0}$ and $\mathbf{Q_0}$ are the $R= [v_k v_k^T]$ and $Q=E[w_k w_k^T]$.

It is important to indicate that we use a n=ndof linear model with m sensors, where m<n. In the algorithm here, it is assumed that the first sensor is placed at the optimal random location and for each single additional sensor the optimal location is estimated. In the first place, consider the equation (2) for the first sensor location

$$\mathbf{0} = \mathbf{AP_1} + \mathbf{P_1}\mathbf{A}^T - \mathbf{P_1}\mathbf{C_1^T}\mathbf{R_0^T}\mathbf{C_1^T}\mathbf{P_1} + \mathbf{Q_0}$$

By adding a new sensor, a new Ricatti equation arise

$$\mathbf{0} = \mathbf{AP_2} + \mathbf{P_2}\mathbf{A}^T - \mathbf{P_2}\,[\mathbf{C_1^T}\mathbf{C_2^T}] \begin{bmatrix} \mathbf{R_1^{-1}} & \mathbf{0} \\ \mathbf{0} & \mathbf{R_2^{-1}} \end{bmatrix} \begin{bmatrix} \mathbf{C_1} \\ \mathbf{C_2} \end{bmatrix} \mathbf{P_2} + \mathbf{Q_0}$$

where $\mathbf{P_2}$is the new steady-state solution

By following the same procedure for every sensor which is adding in the system, the subsequence equation is taken

$$\mathbf{0 = (A - P_1C^TR^{-1}C)\Delta P + \Delta P(A^T - P_1C^TR^{-1}C) - \Delta PC^TR^{-1}C\,\Delta P - P_1C_2^T\,R_2^{-1}C_2P_1} \quad \textbf{(3)}$$

where $\mathbf{\Delta P=P_2 - P_1}$ and $\mathbf{C} = \begin{bmatrix} \mathbf{C_1} \\ \mathbf{C_2} \end{bmatrix}$, $\mathbf{R} = \begin{bmatrix} \mathbf{R_1} & \mathbf{0} \\ \mathbf{0} & \mathbf{R_2} \end{bmatrix}$

Every time where a new measurement is added in the system, the matrix C is estimated. By applying the equation (3), ΔP in the new location of the sensor is calculated and its trace is compared with the trace ΔP of the previous location. The location with the minimum trace of ΔP is retained.

Note that following the aforementioned procedure and solving the equation (3) the possible combinations for the optimal sensor placement are reduced from $\binom{n}{m} = \frac{n!}{m!(n-m)!}$ to $\sum_{i=1}^{m}(n-i)$. It is important to note that the measurement noise in the added sensor must be uncorrelated with the measurement noise in all the initial sensors.

5.1.2. Optimal sensor placement without uncertainties-simulated example

5.1.2.1. A 10-DOF spring-mass model

The second step of this chapter is to present results by changing some important parameters of the system, like the standard deviation of uncertainties and the objective parameter. At first, results for a 10 DOF spring-mass chain-like model without uncertainties are presented. The masses that are used are 0.35 *kg* and the stiffness of the springs is 650 *N/m*. Here, the objective parameter is to minimize the trace of the change in the covariance matrix ΔP. The number of sensors is 5 and the components of the observation noise and the covariance of load are 0.0005 and 10^{-60} respectively. Furthermore one sensor at a time is placed in such a way that the selected position (along with the previously placed sensors) results the minimum trace of ΔP.

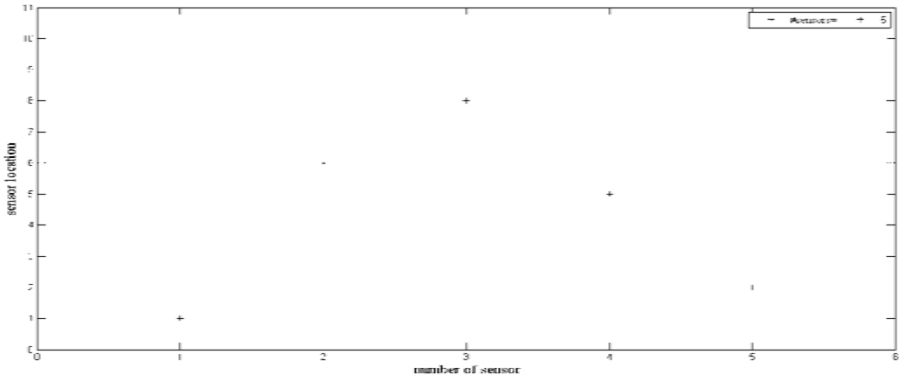

Figure 5.1: the location of the five sensors in the 10 DOF system.

As it is shown in Figure 5.1, the five sensors are located on the 1st, 2nd, 5th, 6th and 8th DOF.

Additionally, the trace (ΔP) is presented bellow for every sensor in the free DOFs. For each sensor the DOF with the minimum trace (ΔP) is selected. The DOF with the minimum trace (ΔP) is underlined with bold. It is assumed that the first sensor is placed always at the 1st DOF.

	1DOF	2DOF	3DOF	4DOF	5DOF	6DOF	7DOF	8DOF	9DOF	10DOF
1st sensor	$-9.7*10^{7}$	-	-	-	-	-	-	-	-	-
2nd sensor	-	7.48	-9.05	-1.36	5.06	**-129**	-31	19	17.4	1.70
3rd sensor	-	-5.8	-10.2	-1.28	-2.85	-	31.1	**-25.7**	11.7	6.99
4th sensor	-	169	-24.3	2.85	**-134**	-	5.20	-	-0.112	-3.26
5th sensor	-	**-1.23**	1.66	0.543	-	-	20.1	-	5.10	-0.75

Table 5.1: optimal sensor placement for five sensors with **objective parameter trace(P_{i+1}-P_i).** All the values are multiplied with 10^{-32}.

It is shown in Table 5.1 that the selected optimal location of one sensor isn't examined as possible optimal location for next sensors. The same thing is done for the first sensor too. For the spring-mass chain like model herein, the first sensor is placed on the 1st DOF, the second sensor on the 6th DOF, the third sensor on the 8th DOF, the fourth sensor is placed on the 5th DOF and finally the fifth sensor is placed on the 2nd DOF.

5.1.2.2. A 40-DOF spring-mass model

Now a 40-DOF system is used in order to show how the trace of the state error covariance P is affected when the number of sensors is increasing. In this section 20 sensors are used. The parameters are remaining the same as in the previous section of this chapter.

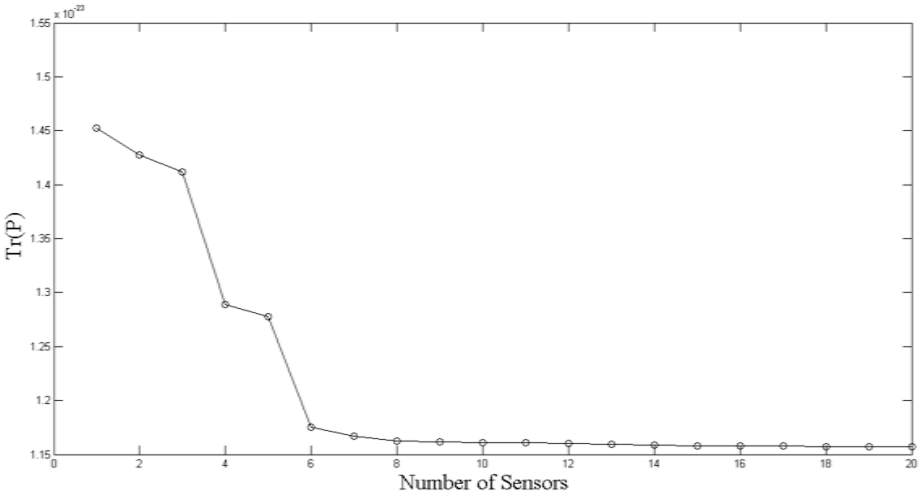

Figure 5.2: The reduction in the trace(P) as a function of the number of sensors.

As it is shown in Figure 5.2, the trace of the state error covariance matrix is reduced when a new sensor is placed in the system. Additionally, it can be noticed that increasing the number of sensors beyond a certain number results that little estimation accuracy is gained

by adding more sensors. The critical number for this simulated example is eight. As a result, it is safe to say that for the certain 40-DOF spring-mass chain-like model the optimal number of sensors that one could use is eight sensors.

5.1.3. Optimal sensor placement with uncertainties-simulated example

The same procedure is followed for the optimal sensor placement with uncertainties. It is decided that the stiffness springs 4 and 8 follow a Gaussian distribution with mean=m=650 and standard deviation s. The samples of uncertainties are 1000. The methodology that is followed remain the same as previous and for all the samples the trace for each added sensor is estimated using the following equation trace(ΔP)= $\sum_{i=1}^{M} tr(\Delta P)_i \, /M$, where M is the number of samples that produced from the Gaussian distribution. Herein, four cases of different standard deviation are studied and results are presented bellow. The **four cases** are i) $s=0*k_0$ ii) $s=0.1*k_0$ iii) $s= 0.2*k_0$ iv) $s=0.3*k_0$.

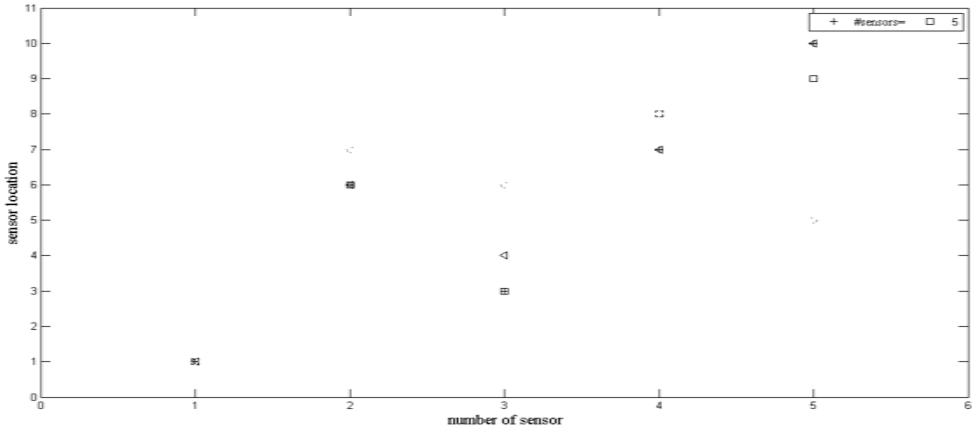

Figure 5.3: the optimal sensor location for each of the 4 cases for 1000 samples, where: **i)=+ ,ii)=square ,iii)=triangle ,iv)=o.**

The Figure 5.3 shows the sensor location for each standard deviation. The four aforementioned groups are:

i) [1 6 3 7 10]

ii) [1 6 3 8 9]

iii) [1 6 4 7 10]

iv) [1 7 6 8 5]

It can be seen that when the standard deviation of the uncertainty is changed, the optimal location for each sensor is also changed. To be more specific, as the standard deviation of the uncertainty is increased, new sensors are located in higher DOFS, except the last one which is located at the fifth DOF. One can seen in Figure 5.3 that for the first three cases the second sensors is placed at the 6^{th} DOF and that the third sensor is placed at lower DOFS.

Also the 4th sensor is placed at the 7th and 8th DOF and the 5th sensor is placed at the 9th and 10th DOF for the first three cases and at 5th for the last case.

5.1.4. Optimal sensor placement with uncertainties and objective det (ΔP)-simulated example

The objective in this part is to demonstrate the results when the objective parameter of the algorithm is the determinant of the ΔP, det (ΔP) and not the trace of ΔP. The same four aforementioned cases of the standard deviation of the uncertainty are used and it was assumed that stiffness of the springs 4 and 8 are uncertain. The results of this analysis are presented beneath.

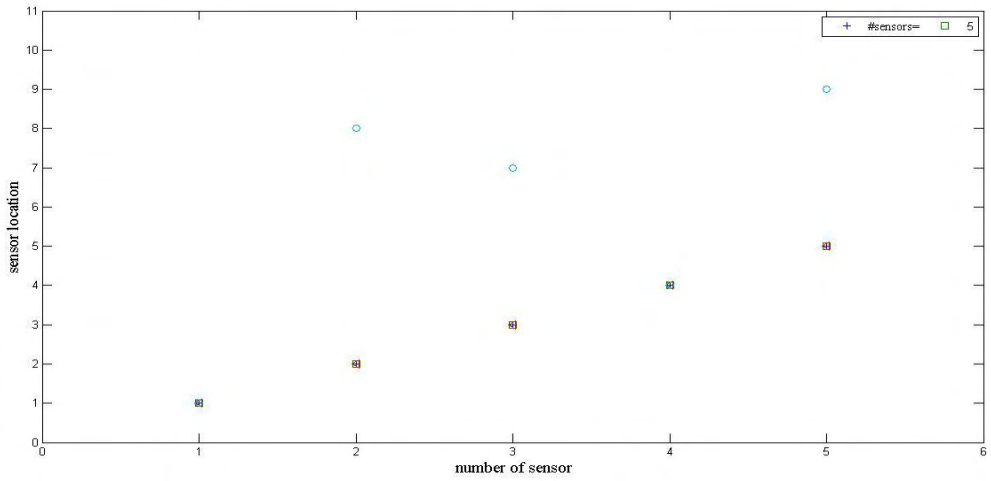

Figure 5.4: the optimal sensor location for each of the four cases for 1000 samples, where: **i)=+ ,ii)=square ,iii)=triangle ,iv)=o.**

It can be seen in Figure 5.4 that the optimal sensor placement for each case is:

i) [1 2 3 4 5], for $s=0*k_0$

ii) [1 2 3 4 5], for $s=0.1*k_0$

iii) [1 2 3 4 5], for $s=0.2*k_0$

iv) [1 8 7 4 9], for $s=0.3*k_0$

For the first three cases, the optimal sensor location for five sensors is exactly the same. Only for standard deviation $s = 0.3*k_0$, the sensors sequence is changed. Note that the fourth sensor is placed on the same location for every standard deviation. In addition, one can notice that the sensors at the fourth case are placed on higher DOFS.

5.2. Optimal sensor placement by using a secondary system

In the previous section of this chapter the optimal sensors' location in a 10 DOF and 40 DOF spring-mass chain-like model was examined and the effects of the model uncertainties on the location of the sensors were studied. In this part of the chapter the primary 10 DOF

spring-mass chain-like model and the secondary 1-DOF spring-mass chain-like model are introduced. The spring's stiffness for the secondary system has the following form

$$\mathbf{K_s = \lambda \omega_1^2 m} \quad \textbf{(1)}$$

where $\boldsymbol{\lambda}$ is a parameter, $\boldsymbol{\omega_1}$ is the minimum eigenvalue of the primary system and **m** is the mass of the secondary system. The secondary system is attached with each location of the primary system and the optimal sensor placement for each location is studied in the following section. By that means, the primary and the secondary system create a general 11 DOF system. In section 5.2.1 a simulated example without uncertainties in stiffness or in λ is presented and the optimal sensor placement for each location of the secondary system in the general system is examined. In section 5.2.2 uncertainties in stiffness of the primary system are inserted and the same procedure as previous is followed. Finally in section 5.2.3, it is assumed that parameter λ follows a Gaussian distribution and the effects of this type of uncertainty on the optimal sensor placement are examined. The objective here is to find how the different locations of the secondary system influence the optimal sensor placement that minimizes the trace of the state error covariance as it was described in the previous section.

5.2.1. Simulated example without uncertainties

Assume that for primary and secondary system the masses are equal to 0.35 *kg*, the springs' stiffness for the primary system is equal to 650 *N/m* and the damping ratio is set 1%. Five sensors are used in the general 11 DOF system and the force is applied to the second DOF of the general system. For this section, it is assumed that λ=1. The objective of this part is to find the optimal sensor placement for 5 sensors for each location of the secondary in the general system without uncertainties in stiffness or in λ parameter. In the following table the optimal sensor placement for the five sensors is presented.

location of the secondary system	Location of the 5 sensors
1	1 2 6 11 9
2	1 6 8 4 9
3	1 7 2 5 9
4	1 9 10 11 6
5	1 7 4 9 6
6	1 10 2 5 8
7	1 2 8 3 7
8	1 10 3 8 4
9	1 2 9 7 4
10	1 10 7 4 3
11	1 5 10 7 8

Table 5.2: optimal sensor placement for each location of the secondary system in the general system.

It can be seen that the different locations of the secondary system affect the optimal sensor placement. It can be noticed that when the secondary system is placed at the 4th DOF, the sensors are located in higher DOFS.

5.2.2. Simulated example with uncertainties in springs' stiffness of the primary system

In this part of the study it is assumed that the stiffness of all the primary system's springs follows a Gaussian distribution with mean=650 *N/m* and standard deviation s=0.1*mean. The objective here is to **minimize** $\sum_{i=1}^{N} \mathbf{P_i/N}$, where N is the number of the stiffness samples which are produced from a Gaussian distribution and P_i is the state error covariance given by the Ricatti equation as it is introduced in section 5.1. For this study the samples number are 100. The secondary system is attached to every one of the 11 DOFS of the general system and the procedure of section 5.2 is followed. The results of the optimal sensor placement are shown in the next table.

Location of the secondary system	Location of the 5 sensors
1	1 9 7 10 4
2	1 2 3 4 11
3	1 8 3 9 7
4	1 6 8 10 4
5	1 10 9 11 2
6	1 7 3 9 10
7	1 8 11 9 2
8	1 9 7 5 4
9	1 4 10 2 9
10	1 10 3 4 8
11	1 3 2 10 9

Table 5.3: optimal sensor placement for each location of the secondary system in the general system.

By seeing the Table 5.3 it is noted that when the secondary system is placed at the 2nd DOF the first four sensors are located on the first four DOFS and the fifth sensor is placed at the last DOF. On the contrary, when the 1-DOF secondary system is placed at the 5th DOF the second, third and fourth sensor is installed at the last three DOFS and the fifth sensor is placed at the 2nd DOF. Also it can be seen that by placing the secondary system at the last DOF the second and the third sensor are installed on the 3rd and 2nd DOF respectively and the two last sensors are placed at the 10th and 9th DOF respectively. Overall, one can notice the inclination of the sensors to be placed at higher DOFS.

5.2.3. Simulated example with uncertainties in parameter λ

The objective in this part is to examine how the uncertainties in parameter λ affect the optimal location of the 5 sensors in the general system. For this, it is assumed that the parameter λ is not known but it follows a Gaussian distribution with mean=1 and standard deviation s=0.1. Defining $\omega_s=\sqrt{\lambda}\omega_1$, where ω_s is the eigenvalue of the secondary system, it is possible to examine the effects that the uncertainties of the parameter λ have on the sensor

location. Additionally, 5 sensors are used and the force is applied to the second DOF of the general system. The model parameters are remaining the same as in paragraph 5.2.1. The results of the optimal sensor location are presented in the next table

Location of the secondary system	Location of the 5 sensors
1	1 9 2 8 4
2	1 6 10 11 9
3	1 2 8 10 9
4	1 8 3 10 4
5	1 11 8 10 2
6	1 10 9 7 2
7	1 3 2 4 5
8	1 3 6 9 10
9	1 10 9 8 7
10	1 11 4 7 6
11	1 9 4 3 2

Table 5.4: optimal sensor placement for each location of the secondary system in the general system.

Table 5.4 shows the optimal sensor placement when uncertainties are inserted in parameter λ. It can be noticed that the fourth sensor is general placed at higher DOFS such as 8, 9, 10 and 11. Additionally one can notice that when the secondary system is placed at the 2, 5, 6 or 9 DOF the sensors are installed on the last degrees of freedom. On the contrary when the 1-DOF system is placed at the 7^{th} DOF, the five sensors are placed at the first five DOFS.

Additionally it is assumed that the secondary system is attached on the 11^{th} DOF of the general system. Using 100 samples from a Gaussian distribution for the parameter λ, four cases for different standard deviation are examined. The four cases are:

- Standard deviation=0.01.
- Standard deviation=0.02.
- Standard deviation=0.05.
- Standard deviation=0.1.

For each of the four cases, the optimal sensor placement is calculate, when the objective function is the trace of ΔP and when the objective function is the determinant of ΔP. The optimal sensors placement for 5 sensors is presented in Table 5.5.

Standard deviation	Objective(trace(ΔP))	Objective(determinant(ΔP))
0.01	1 8 10 11 4	1 2 3 4 8
0.02	1 9 7 10 5	1 2 3 4 8
0.05	1 8 3 6 9	1 2 3 4 8
0.1	1 9 4 3 2	1 2 3 4 8

Table 5.5: Optimal sensor placement for each of the four standard deviation cases.

As it is seen in Table 5.5, when the objective function is to minimize the trace of ΔP, the optimal sensor location is changed for the 4 different standard deviations. It is observed that, when the standard deviation is decreased, the five sensors are located in higher degrees of freedom. On the contrary, when the objective function is to minimize the

determinant of ΔP for each sensor, the optimal sensor placement does not change. In this case can be conclude that the optimal sensor location is not influenced by the change of the standard deviation of the uncertainties in parameter λ.

5.2.4. Conclusion

In this particular chapter the optimal sensor placement was studied. The criterion for the optimal sensor placement was the minimization of the trace or the determinant of the covariance of state error. First the mathematical formula of the sensor's analysis was presented in section 5.1.1. It was shown that solving the Ricatti equation for every sensor which is adding in the system and minimizing the trace of the ΔP it is possible to find the optimal location for every sensor available. Simulated examples using the NDOF spring-mass chain like model were presented. Also by using a 40 DOF spring-mass chain-like model with 20 sensors it was observed that the trace of the state error covariance matrix was reduced when a new sensor was placed in the system. There is a crucial number where the new sensors did not affect the trace of the state error covariance matrix. Afterwards the effects the different kinds of uncertainties have on the optimal sensor placement were studied and analyzed. It was shown that when the standard deviation of the stiffness uncertainty is changed, the optimal locations of the sensors are changed too. Also it was noted that when the objective parameter of the algorithm is the determinant of the ΔP, the different standard deviation did not affect the sensor placement, except the last case, when the standard deviation was $0.3*k_0$. Lastly in section 5.2 a 1-DOF spring-mass secondary system was introduced. It was shown that the different locations of the secondary system in the general system and the uncertainties that were inserted in stiffness and in parameter λ affected the optimal sensor placement. Finally, it was seen that different standard deviations of the uncertainties in parameter λ do not affect the optimal sensor placement when the objective function is the determinant of ΔP. On the contrary, these changes in standard deviation affect the optimal sensor location when the objective function is the trace of ΔP.

CHAPTER 6 The Study of a Lignite Grinder Assembly Base in a Power Plant

6.1 Introduction

The effectiveness of the dual Kalman filter that was presented in Chapter2 is checked, by applying it to a more complex mechanical system. The mechanical system is a lignite grinder assembly base that it is used to support the lignite grinder assembly in the power plant of the city of Florina, Greece. The upper part of the base is connected with a metallic bearing box and a metallic shaft. The shaft is rotating with different speeds and it is swaying the base. Due to this oscillation, the base is suffering from damage accumulation and it fails. The geometrical shape of the base is presented in Fig 6.1. The main base includes a lower and an upper base. In order to measure the acceleration time histories, 10 sensors are used and placed in different locations on the base. Four of the sensors are placed at the lower base, four on the upper base and the two remaining are placed on locations at the upper base where the base is connected with the bearing box. Specifically, the points 1, 2, 3, 4 are the four points of the lower base which is located to the ground. The points 5, 6, 7, 8 are placed to the beams which support the bearing box and the base. Finally the points 9 and 10 support the bases' setscrew that connects the base and the bearing box. Each point includes three DOFS, each for one of the three dimensions x, y, z.

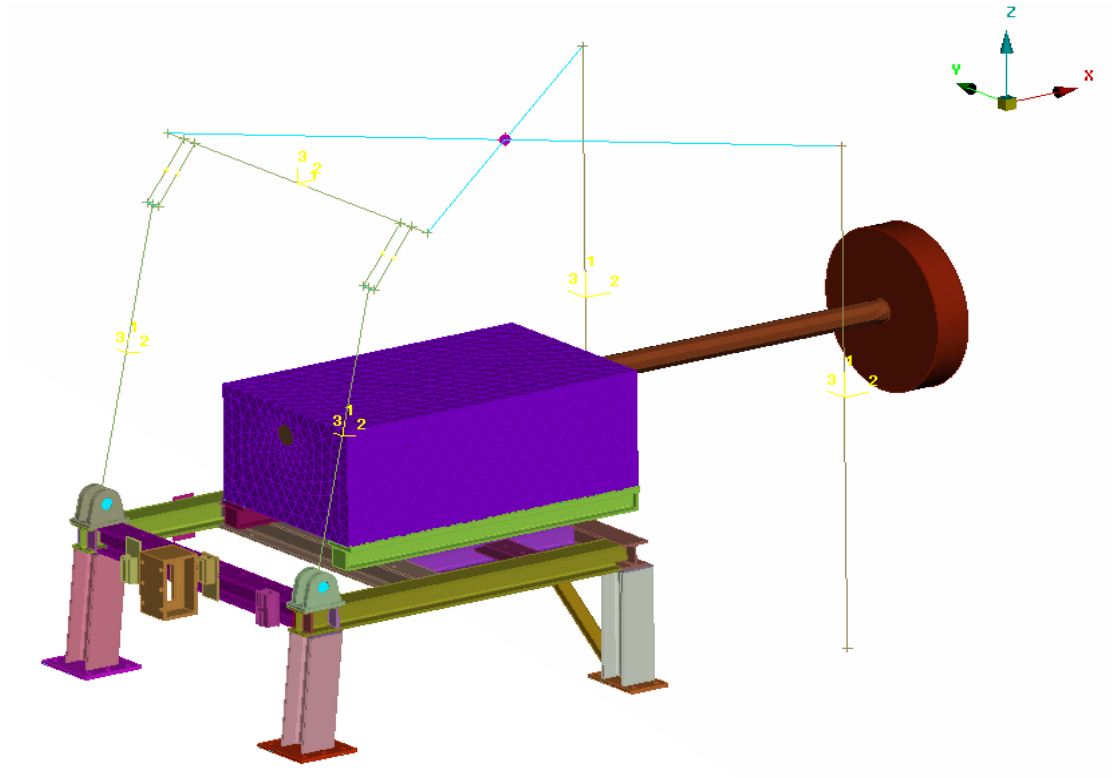

Figure 6.1: the metallic base of the Meliti power plant.

The metallic base that is studied is a complex structure, so sophisticated numerical models such as Finite Elements are used in order to calculate and calibrate the matrices for stiffness, mass and damping. Accurate finite elements are very important nowadays, since they are

used in the dynamic design of the structures in computer level and saving time and money. The measurements and the discrete FE model is based on the work of Prof. D. Giagkopoulos et all [32]. Here the assumption is made that in the lower base there are four springs with very big stiffness value and that unknown forces are applied on the points where measurements are taken.

6.2 Predictions using real-life acceleration measurements

Using the acceleration measurements from 8 sensors the DKF is used in order to predict the acceleration time histories all over the system and find the unknown forces. It is assumed that the unknown forces are applied to the DOFS where measurements are taken. The number of freedom for this model is 105 and the damping ratio is chosen 1%. The L-curve technique is used in order to tune the covariance of state and noise. Additionally the observation noise covariance matrix is tuned by following the tuning technique from section 2.8. Note that there are many sources of force in the system which are not taken into consideration. In the following figures the predicted acceleration time histories of some DOFS of the system where measurements are taken are presented. The first three DOFS are located on the lower basis and the other three DOFS are located on the upper basis.

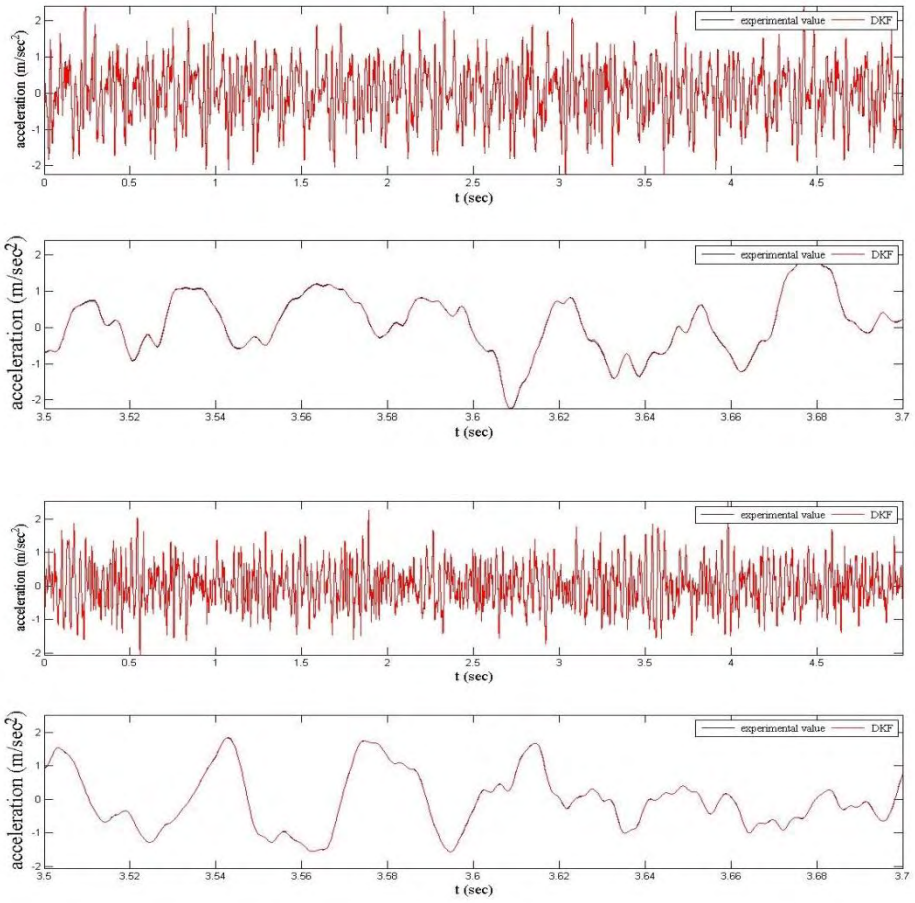

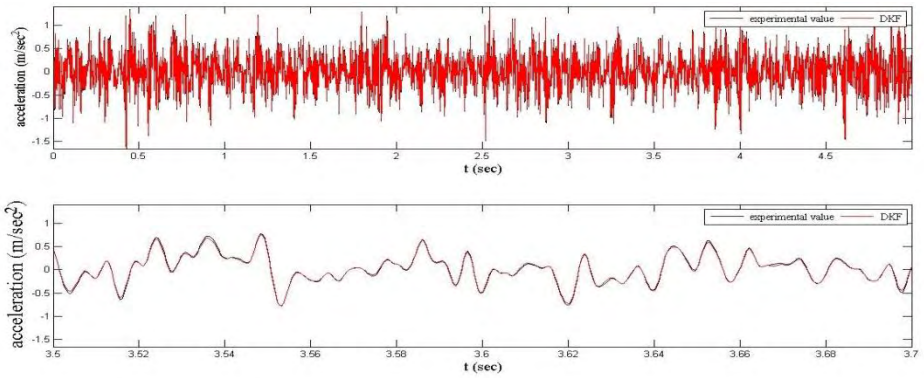

Figure 6.2: Predicted and measured acceleration time histories for 3 DOFS of the lower base.

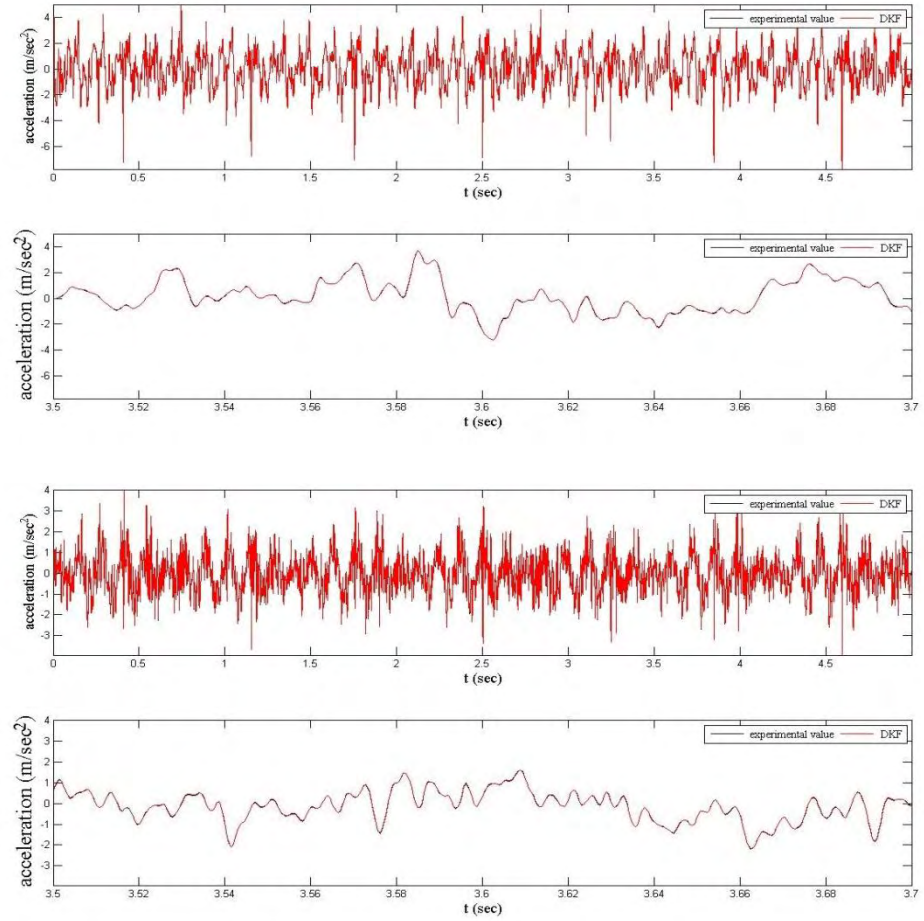

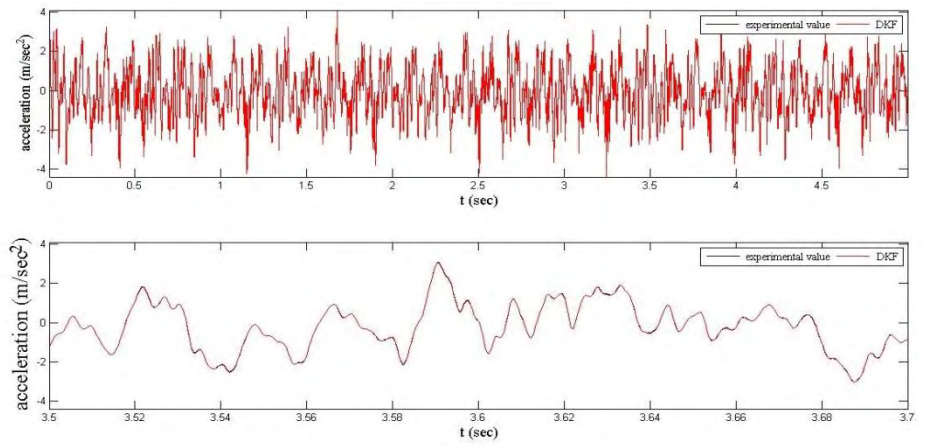

Figure 6.3: Predicted and measured acceleration time histories for 3 DOFS of the upper base.

In Figure 6.2 and 6.3 can be seen that using the DKF procedure the predicted acceleration time histories for the measured DOFS are very accurate. It seems that the dual Kalman filter works excellent for the acceleration prediction of the measured DOFS. As it is said above, the L-curve technique is used in order to tune properly the covariance matrix of state and load. The L-curve for all the acceleration measurements of the system is presented in the following figure. The diagonal components of the covariance of state are set 10^{-5}.

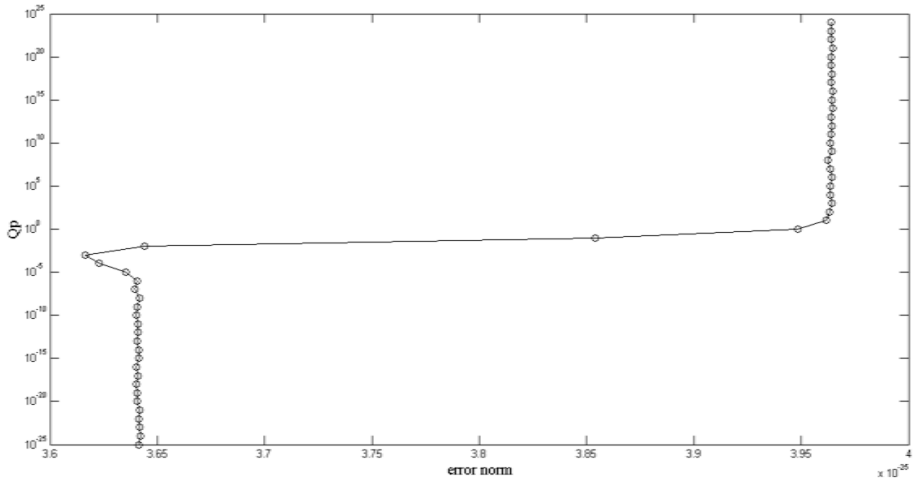

Figure 6.4: L-curve technique for all the measurements of the system.

It seems that the error between the measured and the predicted acceleration time histories for the points where measurements are taken is minimized to the value of 10^{-25}. The values of the diagonal components of the covariance of load for perfect accuracy when the covariance of state is 10^{-5} are set 10^{-3}. In previous chapter it was seen that if the predictions of the acceleration time histories has perfect accuracy, the predicted displacement time histories are not so accurate. Hence, in order to take good predictions for acceleration and displacement time histories, the diagonal components of the covariance of state and load are set 10^{-22} and 10^{-3} respectively.

The previous predictions are done using the M-K-C matrices. As it is said in previous chapter, it is possible to use the modal analysis and take the same predictions from the DKF. In Figure 6.5 it is proved that the predictions using the M-K-C and modal analysis give exactly the same results.

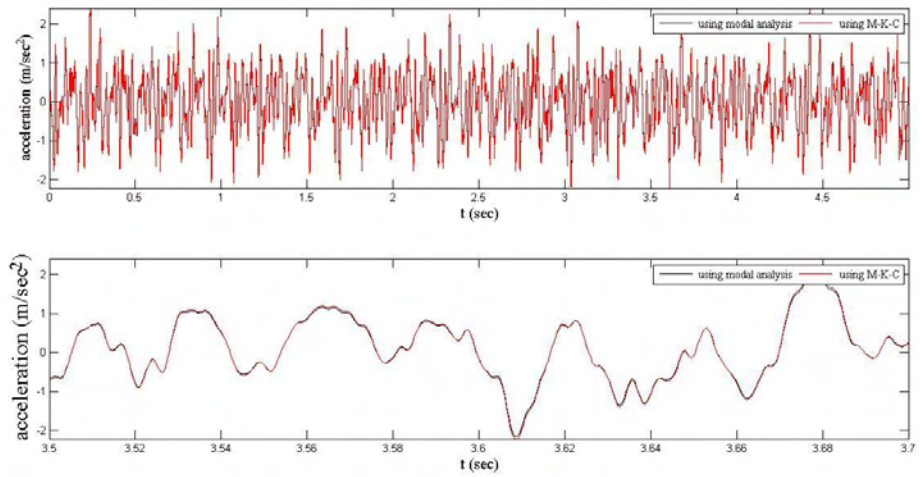

Figure 6.5: Comparison between the modal analysis and M,K,C analysis for a certain DOF of the lower base.

In Figure 6.4 the predicted acceleration time history that it is calculated for a certain DOF of the system is exactly the same using modal analysis and M-K-C analysis. The differences here are minimized.

As it was said above, unknown forces are applied on the DOFS where acceleration measurements are taken. Using the DKF it is possible to find these unknown forces. By finding an average for the predicted forces of the lower base and an average for the predicted forces of the upper base it is possible to find where the unknown forces are maximized.

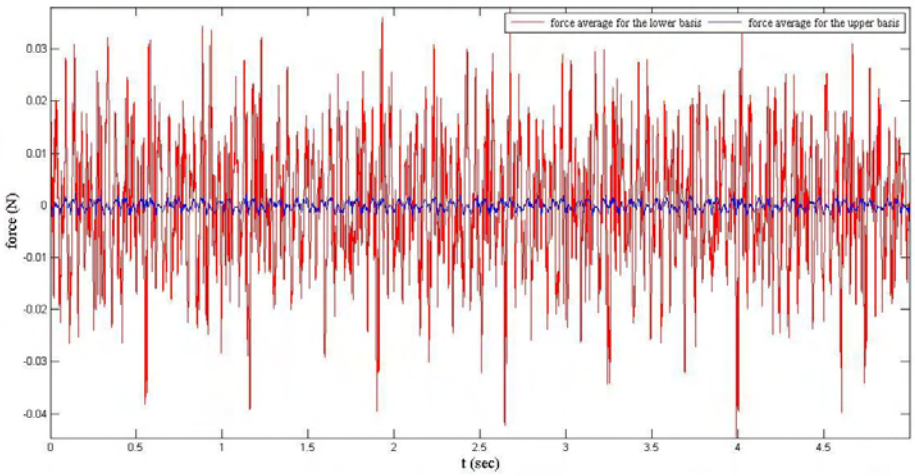

Figure 6.6: An average prediction of the unknown forces for the lower and upper base.

In Figure 6.6 it is observable that the forces that applied on the upper base are smaller than the forces that applied on the lower base.

In the Figures 6.7 & 6.8 the predicted acceleration time histories for six unmeasured DOFS are presented, three for each point. The points 9th and 10th are studied. These points are located to the upper base. Also a comparison is made between the acceleration measurements and acceleration predictions for these points in order to see how accurate the model is.

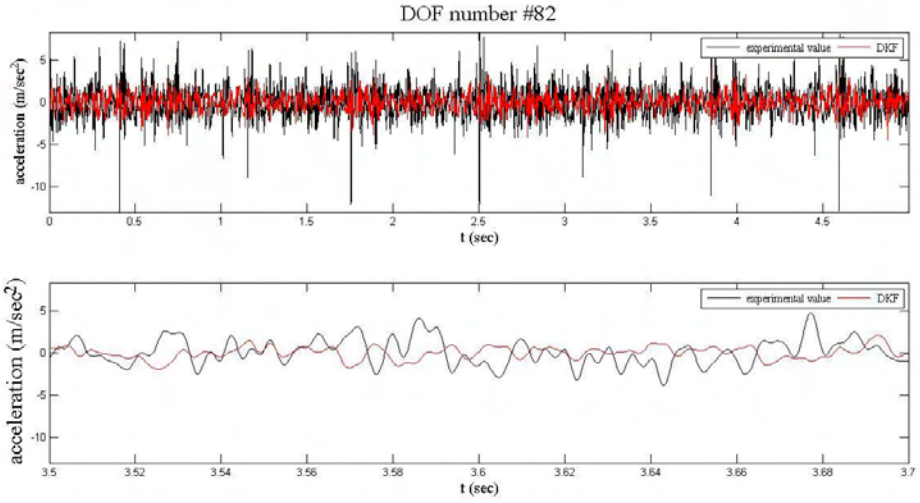

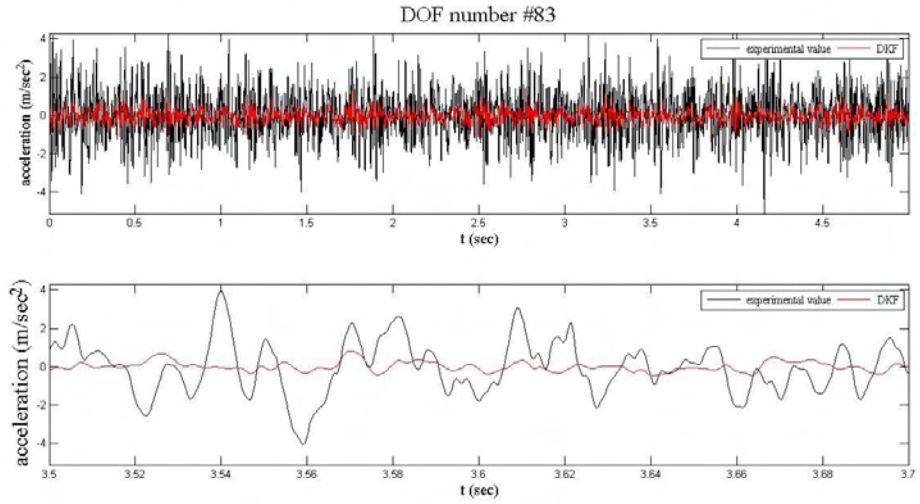

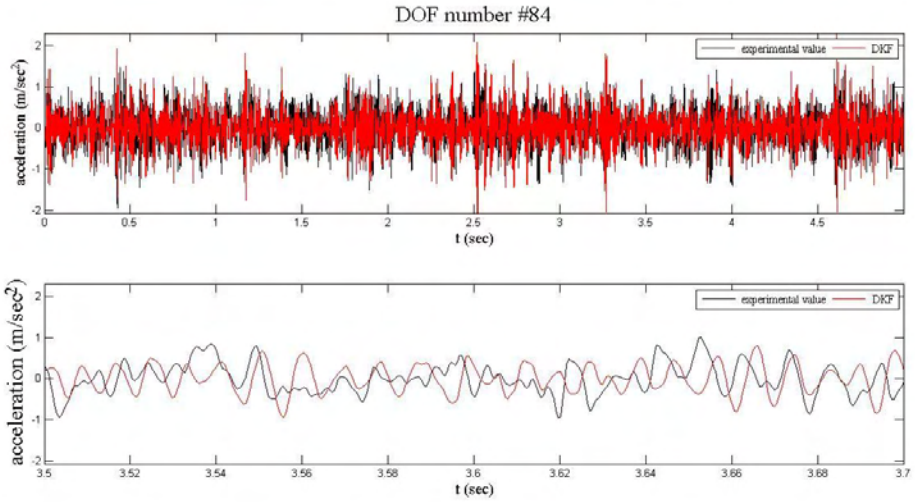

Figure 6.7: Acceleration predictions for the 9th point which include the 82, 83 and 84 DOFS.

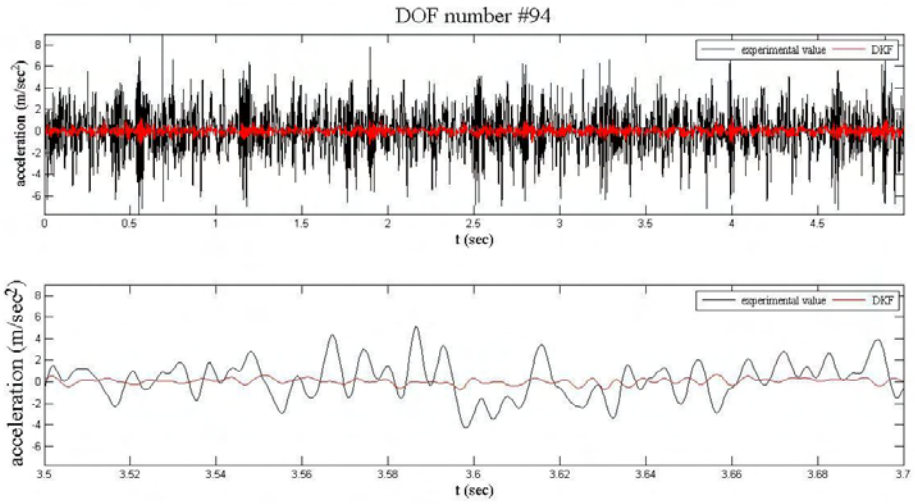

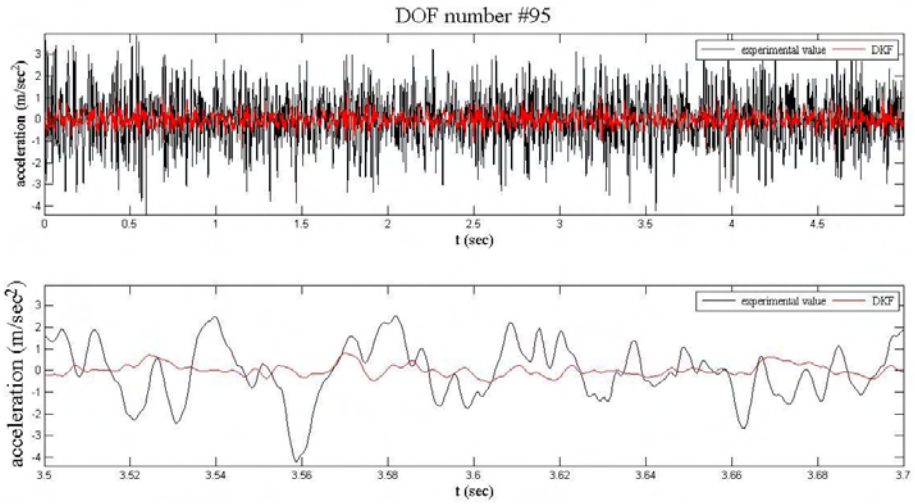

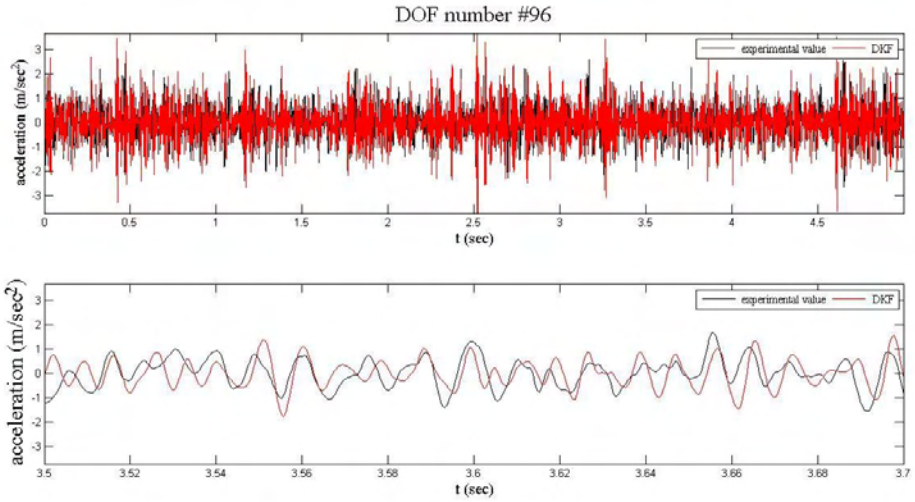

Figure 6.8: Acceleration predictions for the 10th point which include the 94, 95 and 96 DOFS.

In Figures 6.7 and 6.8 can be seen that most of acceleration predictions are not accurate. This is due to the fact that maybe the model is inappropriate for the DKF procedure, or it is insufficient. By choosing a more sufficient model, it is expected to take very good predictions for the unmeasured points. In the following section the acceleration measurements are taken through simulated experiments.

6.3 Predictions using simulated experiments

In this section the acceleration measurements from the real-life sensors are now used in order to produce simulated acceleration measurements. The model that it is used is the same with the model in the previous section. The diagonal components of the covariance matrices of state and load are set 10^{-60} and 10^{-3} respectively and the observation covariance matrix is chosen 1% of the acceleration peak. It is assumed that the unknown forces are applied on the DOFS where measurements are taken. By using the DKF procedure the predicted acceleration and displacement time histories for the unmeasured DOFS are presented in Figures 6.9 & 6.10.

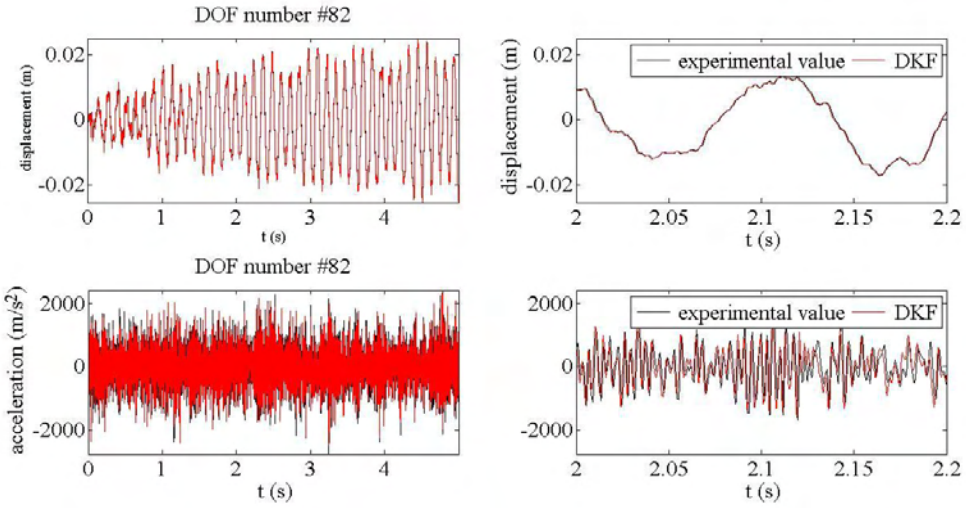

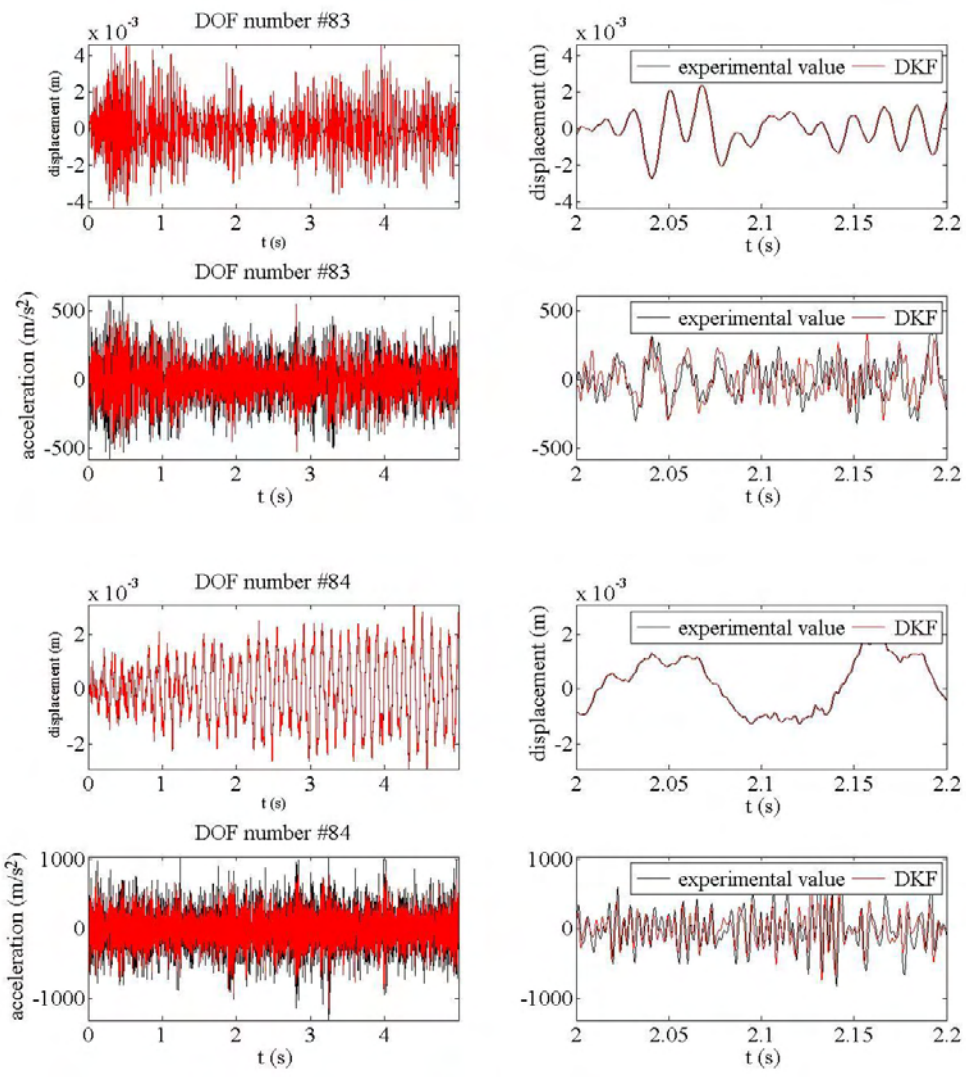

Figure 6.9: Acceleration and displacement time histories using DKF for the 9th point.

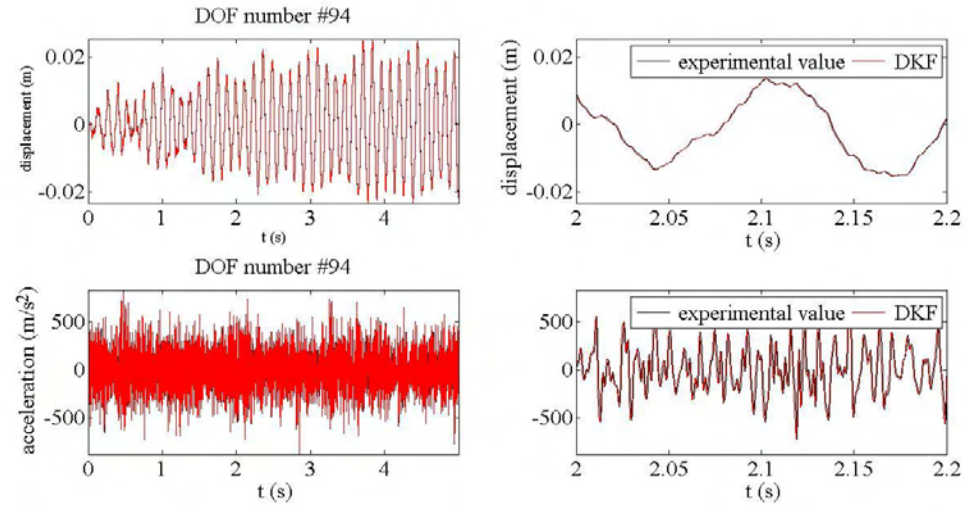

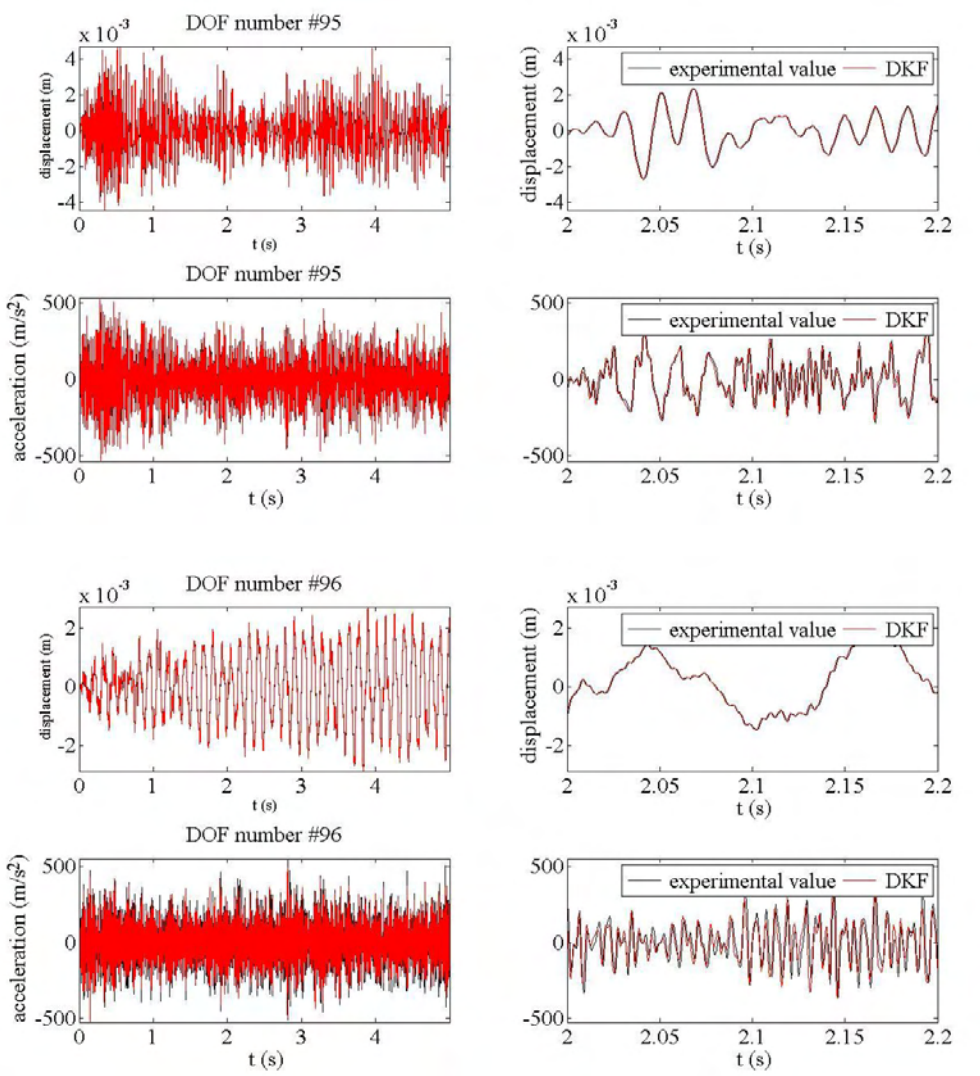

Figure 6.10: Acceleration and displacement time histories using DKF for the 10th point.

It can be seen in Figures 6.9 and 6.10 that the predicted acceleration and displacement time histories are very accurate. By choosing appropriate values for the covariance of state and input it is possible to take perfect predictions for the acceleration time histories. On the contrary in this simulated example the covariance of state and input are chosen in order to take perfect predictions for the displacement time histories and very good predictions for the acceleration time histories.

6.4 Conclusions

In this chapter a study is done in order to predict the acceleration and displacement time histories of a metallic base. In the first section of this chapter it is assumed that acceleration measurements are taken from a limited number of sensors that are attached at some points of the base. Using the DKF predictions are made for the acceleration, displacement and force time histories at selected locations of the metallic structure. It is found that the accelerations predictions for the measured points have perfect accuracy. On the contrary, the predictions for the unmeasured points are much less accurate. This is due to the fact that this certain model used is not accurate enough for this DKF procedure. In the section

6.3 the acceleration measurements taken from the sensors are used in order to produce new acceleration measurements through a simulated generator program. The model that it is used remains the same. It is found that by tuning the covariance matrices of load and state with the appropriate values it is possible to make perfect predictions for the acceleration and displacement time histories.

CHAPTER 7 Conclusions & Future Work

7.1 Conclusions

In this diploma thesis a dual implementation of the Kalman filter, namely the DKF is applied. At first, the DKF methodology was applied for a simple spring-mass chain like model. By using the DKF, it was possible to find the acceleration and displacement time histories all over the system, using measurements from few DOFS. Also the unknown force time history was calculated from the dual Kalman implementation. It is important to note that the acceleration or the displacement measurements was produced from a simulated experiment. The linear dynamics problem was solved using two methodologies. First, the matrices M, K, C were used in the DKF analysis and results are taken. The second way to solve the problem is the modal analysis. By using the normalized eigenvectors, the eigenvalues and the damping ratio it was shown that is possible to take the same results as the first methodology. Furthermore, by utilizing the modal analysis it is feasible to use few modes in the DKF analysis. That makes the analysis faster and simpler. Additionally the tuning of the covariance matrices was studied and methodologies are examined. The L-curve technique was shown to be very accurate for the estimation of the covariance of input. Also a methodology was studied in order to tune the diagonal components of the observation noise covariance.

Next the stiffness uncertainties in the prediction of the acceleration, displacement and force time histories using DKF were studied. Uncertainties may arise in the system due to assumptions that are done in order to construct the model. By assuming that the stiffness uncertainties follow a Gaussian distribution, it was observed that they play an important role in the prediction of the performance and safety of structural systems. Furthermore using the quartile theory boundaries are set in order to show how small are the divergences between the experimental and the predicted acceleration and displacement time histories. These boundaries are created using the samples of stiffness uncertainties. The results that were taken show that the experimental time histories are inside the 5% and 95% boundaries.

In Chapter 4 linear damage accumulation law, Rainflow cycle-counting algorithms and S-N fatigue curves are used in order to predict the fatigue damage accumulation of a spring-mass chain like model. Stress time histories for all the hotspots of the model were calculated using the predicted displacement time histories from the DKF. These stress time histories are used in the program in order to predict the fatigue damage accumulation all over the system. As a result, it was possible to find which spring suffers the most from damage. Additionally the effects that model uncertainties have on the fatigue damage accumulation were examined. It was assumed that stiffness uncertainties were inserted in some springs of the system. It was shown that if the uncertainties follow a Gaussian distribution, the fatigue damage accumulation for this particular spring seems like a Gaussian curve. When the number of the uncertainty's samples which are produced from a Gaussian distribution is increased, the aforementioned fatigue damage curve can be adequately represented by a Gaussian distribution. Also the fatigue damage accumulation and fatigue lifetime for two

samples of a spring with stiffness uncertainties was presented. It was observed that the fatigue damage is more important in the area where the force was applied. Finally it was shown that the fatigue damage accumulation does not follow the increased or decreased trend of the samples of the spring's stiffness and it is completely independent. The methodology which is used in this chapter could be a very useful tool for the prognosis of the damage in many metallic structures such as buildings, ships, steel bridges, turbines etc.

The optimal sensor placement was also studied in Chapter 5. By solving the Ricatti equation for the change of the covariance matrix ΔP for each adding sensor and minimizing the trace of the ΔP, it was possible to find the optimal sensor location for a spring mass chain like model. Also it was proved that the trace of the state error covariance matrix is reduced when a new sensor is placed in the system and that there is a critical number of sensors after which little estimation accuracy is gained by adding new sensors. Furthermore model uncertainties of the stiffness were studied and the effects on the optimal sensor placement were examined. It was observed that when the standard deviation of the stiffness uncertainty changed in the case that the objective function is the trace of ΔP, the optimal sensor placement changed too. On the contrary, when the objective function was the determinant of ΔP, the optimal sensor placement did not change for the first three cases of standard deviation of uncertainty.

In the second part of Chapter 5 a passive system was introduced. It was assumed that the general system contained a 10-DOF spring mass system which was called the primary system and a 1-DOF spring mass system which was called the secondary system. By locating the secondary system in every DOF of the primary system it was possible to examine how the different locations of the secondary system affect the optimal sensor placement. It was observed that sensors were placed in the highest DOFS of the general system. Moreover it was assumed that uncertainties were inserted in the stiffness of some springs and in the parameter λ which it defined the eigenvalue of the secondary system. The results that were taken are presented and studied in Chapter 5, section 5.2.2 & 5.2.3. Finally, it was seen that different standard deviation of the uncertainty in parameter λ does not affect the optimal sensor placement when the objective function is the determinant of ΔP. On the contrary, these changes in standard deviation affect the optimal sensor location when the objective function is the trace of ΔP.

Finally, in Chapter 6 a metallic base from Meliti PPC power plant was studied and predictions are done. First it was assumed that acceleration measurements were taken from sensors that were located on different hotspots of the base. It was found that acceleration predictions for the measured points of the structure have 100% accuracy and for the unmeasured points the predictions were less accurate. On the contrary, by using the real acceleration measurements in order to produce new measurements from a simulated generator program, it was found that it is possible to make very good predictions for the acceleration and displacement time histories.

Summarizing the current diploma thesis, the contributions are the following:

- An automatic procedure is proposed for predicting the fatigue accumulation of any metallic structure using acceleration measurements from a limited number of sensors.
- Methodologies for tuning the covariance matrices of observation noise, input and state are proposed.
- The DKF is modified in order to take acceleration and displacement predictions all over the structure using acceleration and displacement measurements from a limited number of locations.
- The effects of the stiffness uncertainties on the prediction of acceleration, displacement, force time histories and on the fatigue damage accumulation for a spring-mass chain like model are studied.
- The effects of different kinds of uncertainties on the optimal sensor placement are examined.
- The optimal sensor placement when the objective is the determinant of ΔP is studied.
- Methodologies where the optimal number of sensors is decided.
- How the secondary 1-DOF spring-mass system and his uncertainties in parameter λ and stiffness affects the optimal sensor placement if it is placed in different position of the primary system.
- The DKF is used to make predictions for a more complex metallic structure.

7.2 Future Work

The developed strategies and issues of this thesis certainly open the door for future research activities. An interesting issue that is not investigated in the context of this thesis is how to connect the optimal sensor placement technique that is discussed in this diploma thesis with the DKF procedure. By doing that, it will be possible to achieve great prediction and perfect accuracy. Another recommendation for future work could be the study of new tuning techniques (concerning the model and the measurements) for the optimal predictions of acceleration and displacement time histories using the DKF. Finally, a very interesting issue is to modify the DKF procedure in order to use known and unknown input force and make predictions for acceleration, displacement and unknown force time histories.

References

[1] Saeed Eftekhar Azam, E. Chatzi, C. Papadimitriou, A dual Kalman filter approach for state estimation via output-only acceleration measurements, Mechanical Systems and Signal Processing (2015)1-21.

[2] E. Lourens, E. Reynders, G. De Roeck, G. Degrande, G. Lombaert, An augmented Kalman filter for force identification in structural dynamics, Mech. Systems and Signal Processing 27 (2012) 446-460.

[3] C. Papadimitriou, C. P. Fritzen, P. Kraemer, E. Ntotsios, Fatigue predictions in entire body of metallic number of vibration sensors using Kalman filtering, Struct. Control Health Monit. 18 (2011) 554-573.

[4] J. Ching, J. L. Beck, Real-time reliability estimation for serviceability limit states in structures with uncertain dynamic excitation and incomplete output data, Probab. Eng. Mech. 22 (2007) 50-62.

[5] S. Gillijns, B. De Moor, Unbiased minimum-variance input and state estimation for linear discrete-time systems, Automatica 43 (2007) 111-116.

[6] S. Gillijns, B. De Moor, Unbiased minimum-variance input and state estimation for linear discrete-time systems with direct feedthrough, Automatica 43 (2007) 934-937.

[7] S.Bittanti, S. M. Savaresi, On the parameterization and design of an extended Kalman filter frequency tracker, IEEE Trans. Autom. Control 45 (2000) 1718-1724.

[8] M.R. Rajamani, J. B. Rawlings, Estimation of the disturbance structure from data using semidefinite programming and optimal weighting, Automatica 45 (2009) 142-148.

[9] C. Papadimitriou, G. Lombaert, The effect of prediction error correlation on optimal sensor placement in structural dynamics, Mech. Syst. and Signal Process. 28 (2012) 105-127.

[10] K. Sobczyk, B. F. Spencer, Random Fatigue: From Data to Theory, Academic Press, INC., Harcourt Brace Jovanovich, Publishers (1992).

[11] Saeed Eftekhar Azam, E. Chatzi, C. Papadimitriou, A. Smyth, Experimental validation of the Kalman-type filters for online and real-time state and input estimation, Journal of Vibration and Control (2015) 1-26.

[12] R. A. Khoraskani, M. Mofid, S. Eftekhar Azam, M. E. Hassanabadi, A new simplified formula in prediction of the resonance velocity for multiple masses traversing a thin beam, Scientia Iranica A (2016) 23(1), 133-141.

[13] J. M. Tunna, Fatigue life prediction for Gaussian random loads at the design stage, Fatigue Fract. Engng Mater. Struct. Vol. 9, No. 3 (1986), 169-184.

[14] E. Lourens, C. Papadimitriou, S. Gillijns, E. Reynders, G. De Roeck, G. Lombaert, Joint input-response estimation for structural systems based on reduced-order models and vibration data from a limited number of sensors, Mech. Syst. and Signal Process. 29 (2012), 310-327.

[15] C. Stephan, Sensor placement for modal identification, Mech. Syst. and Signal Process. 27 (2012), 461-470.

[16] Z. Gajic, Introduction to linear and nonlinear observers, Rutgers University

[17] G. Welch, G. Bishop, An introduction to the Kalman Filter, University of North Carolina at Chapel Hill, Siggraph 2001.

[18] C. Papadimitriou, Optimal sensor placement methodology for parametric identification of structural systems, Journal of Sound and Vibration 278 (2004) 923-947.

[19] D.C. Papadioti, Management of uncertainties in structural response and reliability simulations using measured data, Thesis for the degree of Doctor of Philosophy (2015).

[20]F.E. Udwadia, Methodology for optimal sensor locations for parameter identification in dynamic systems, American Society of Civil Engineers, Journal of Engineering Mechanics 120 (2) (1994) 368–390.

[21] Eric M. Hernandez, Efficient optimal sensor placement for state estimation in structural dynamics, Mechanical Systems and Signal Processing (2016).

[22] C.Papadimitriou, E. Lourens, G. Lombaert, G. De Roeck, Kai Liu, Prediction of fatigue damage accumulation in metallic structures by the estimation of strains from operational vibrations.

[23] S. E. Azam, M. Mofid, R. A. Khoraskani, Dynamic response of Timoshenko beam under moving mass, Scientia Iranica (2013).

[24] S. Sankararaman, Y. Ling, C. Shantz, S. Mahadevaz, Uncertainty quantification in fatigue damage prognosis, Annual Conference of the Prognostics and Health Management Society (2009).

[25] V.K. Dertimanis, E.N. Chatzi, S. Eftekhar Azam, C. Papadimitriou, Fatigue assessment in steel railway bridges using output vibration measurements and partial structural information, Proceedings of the Third International Conference on Railway Technology-paper 139, (2016).

[26] T. Kontoroupi, A. Smyth, Online noise identification for joint state and parameter estimation of nonlinear systems, ASCE-ASME Journal of Risk and Uncertainty in Engineering Systems, Part A civil Engineering, Vol. 2, Issue 3 (2015).

[27] M.A. Miner, Cumulative damage in fatigue, Applied mechanics Transactions (ASME) 12 (3): A159-A164 (1945).

[28] A. Palmgren, Die Lebensdauer von Kugallagern, VDI-Zeitschrift 68(14):339-341 (1924).

[29] I.B. Buckle, Passive control of structures for seismic loads, Dept of Civil Engineering, University of Nevada-Reno, 12WCEE (2000).

[30] Prof. C. Papadimitrious' notes about passive systems and uncertainties in fatigue.

[31] S. Mariani, A. Ghisi, Unscented Kalman filtering for nonlinear structural dynamics, Nonlinear Dyn. 49 (2007) 131-150.

[32] D. Giagopoulos, A. Arailopoulos, S. E. Azam, C. Papadimitriou, E. Chatzi, K. Grobanopoulos, Dynamic Response Estimation and Fatigue Prediction in a Linear Substructure of a Complex Mechanical Assembly, Proceedings of 8th European Workshop on Structural Health Monitoring (EWSHM 2016), July 5-8, 2016, Bilbao, Spain, 2016.